Pyramidal Heteroanion-directed and Reduced Mo^{V}-driven assembly of Multi-layered Polyoxometalate Cages

Qi Zheng,[a] Manuel Kupper,[a] Weimin Xuan,[a] Hirofumi Oki,[b] Ryo Tsunashima,[b] De-Liang Long[a] and Leroy Cronin[a]

Abstract: The fabrication of redox-active polyoxometalates (POMs) that can switch between multiple states is critical for their application in electronic devices, yet, a sophisticated synthetic methodology is not well developed for such cluster types. Here we describe the heteroanion-directed and reduction-driven assembly of a series of multi-layered POM cages **1**-**10** templated by 1-3 redox-active pyramidal heteroanions. The heteroanions greatly affect the self-assembly of the resultant POM cages, leading to the generation of unprecedented three-layered peanut-shaped - **4**, **7** and **8** - or bullet-shaped - **5** and **6** - structures. The introduction of reduced molybdate is essential for the self-assembly of the compounds and results in mixed-metal (W/Mo), and mixed-valence (W^{VI}/Mo^{V}) **1**-**10**, as confirmed by redox titration, UV-Vis-NIR, NMR spectroscopy and mass spectrometry. **11**, the tetrabutyl ammonium (TBA) salt derivative of the fully oxidized **3**, is produced as a model structure for measurements to confirm that **1**-**10** are a statistical mixture of isostructural clusters with different ratios of W/Mo. Finally, multi-layered POM cages exhibit dipole relaxations due to the presence of mixed valence W^{VI}/Mo^{V} metal centers, demonstrating their potential uses for electronic materials.

The emergence of energy-related catalysis and electronic device designs demand new metal oxide materials with specific chemical compositions and structures.[1] Polyoxometalates (POMs) are a unique class of discrete molecular metal-oxides with a diversity of structures and properties, which can fulfil this urgent requirement.[2] As an important subclass, heteropolyoxometalates (HPOMs) - generally templated by heteroanions (HAs) with a variety of geometries - have attracted wide attention in recent years owing to their structural diversities and stabilities, rich electrochemistry, and appealing catalytic activities.[3] In particular, incorporation of pyramidal redox-active HAs into HPOMs not only leads to the discovery of a series of unconventional Dawson-type HPOMs, but also allows the facile tuning of redox properties arising from the intramolecular electronic interactions between encapsulated HAs and the metal oxide framework.[4] So far, pyramidal $[XO_3]^{2-}$ HAs have been successfully incorporated into peanut-shaped Dawson-like clusters $[M_{18}O_{54}(XO_3)_n]^{4-/8-}$ (n=1, 2; X= As, Bi, S, Se, HP, etc.) [5] and "Trojan horse"-type clusters $[W_{18}O_{56}(XO_3)_2(H_2O)_2]^{8-}$ (X=S, Se or HP).[5a, 6] The oxidation of redox-active HAs couples with reversible multi-electron transfer to the metal oxide shells of HPOMs, resulting in interesting thermochromic behavior, structural transformation to a conventional Dawson cluster, and application in a flash memory architecture.[4b, 6] As such, it would be of interest to further develop HPOM cages incorporating multiple pyramidal HAs, enabling the potential manipulation between multiple states based on the redox behaviour of the HAs. Although multi-layered $\{M_{30}O_{90}\}$ (M=W or Mo) clusters, incorporating both pyrophosphate and pyramidal HAs, have been reported, a general synthetic strategy is not yet developed for the assembly of such clusters based solely upon pyramidal HAs.[7]

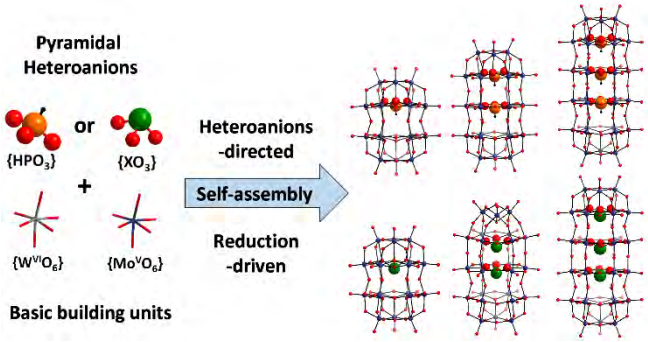

Scheme 1. Schematic representation of pyramidal heteroanion-directed and reduced Mo^{V}-driven assembly of multi-layered POM cages. Colour scheme: orange: P; green: Se; indigo: W/Mo^{V}; red: O; black: H.

In POM chemistry, reduction is well-known for its key role in directing the self-assembly of POM clusters, as exemplified by the reduction-driven formation of giant molybdenum blue (MB) clusters,[8] including wheel-shaped $\{Mo_{154}\}$, $\{Mo_{176}\}$, blue "lemon" $\{Mo_{368}\}$, and molybdenum brown sphere $\{Mo_{132}\}$.[9] In the presence of HAs, partial reduction of the molybdate has led to the isolation of a sulfite templated mixed-valence $[Mo^{VI}_{16}Mo^{V}_{2}O_{54}(SO_3)_2]^{6-}$ cage.[12] However, in constrast to the polyoxomolybdates mentioned above, reduced polyoxotungstates (POTs) are very labile and easily reoxidized to their fully-oxidized forms, preventing further assembly into larger architectures. However, combining reduced molybdate $[Mo^{V}_{2}O_4(H_2O)_2]^{2+}$ with tungstate led to the discovery of a mixed-metal analogue $\{W_{72}{}^{VI}Mo^{V}_{60}\}$ of spherical $\{Mo_{132}\}$, indicating the potential for introducing reduced Mo species in promoting the formation of novel POT clusters.[10]

In this work we demonstrate a strategy to produce muti-layered HPOMs by introducing reduced Mo as a heterometal, resulting in a series of mixed-metal and mixed-valence (W^{VI}/Mo^{V}) POM clusters, **1-10**, templated by $[XO_3]^{2-}$ (X=HP, Se, Te) HAs. All obtained compounds exhibit cage-like frameworks consisting of 2-4 metal layers and 1-3 HAs. Compounds **1**-**3** share the same two-layered peanut-shaped framework, templated by three types of HAs, respectively (Figure 1a). Compounds **4**-**6** feature unprecedented three-layered cage structures, while **7** and **8** exhibit unique three-layered cages,

[a] Dr. Q. Zheng, M. Kupper, Dr. W. Xuan, Dr. D.-L. Long, Prof. Dr. L. Cronin
WestCHEM, School of Chemistry
The University of Glasgow
Glasgow G12 8QQ (UK)
E-mail: Lee.Cronin@glasgow.ac.uk
Homepage: http://www.croninlab.com
[b] H. Oki, Dr. R. Tsunashima,
Graduate School of Sciences and Technology for Innovation,
Yamaguchi University
Yoshida 1677-1, Yamaguchi, 753-8512, Japan

Supporting information for this article is given via a link at the end of the document.

templated by mixed HAs (Figure 2). Compounds **9** and **10** present four-layered cage structures similar to the reported $\{M_{30}O_{90}\}$ but, here, are solely constructed from pyramidal HAs (Figure 3).[7] Compound **11** is the cation-exchanged, TBA salt, derivative of **3** in its fully-oxidized state. All compounds were characterized crystallographically and the formula assignments are supported by an extensive array of analytical techniques (see Supporting Information).

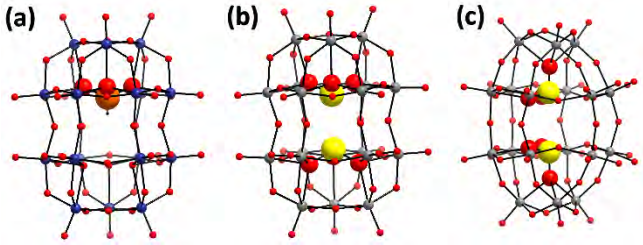

Figure 1. Structural representations of a) $[W^{VI}_{16}Mo^{V}_{2}O_{54}(XO_3)]^{10-}$ (X=HP for **1**, X=Se for **2**, X=Te for **3**). b) peanut-shaped cluster $[X_2W_{18}O_{60}]^{4-}$ (X=S, Se).[5a, 6b] c) "Trojan-Horse" type clusters $[W_{18}O_{56}(XO_3)_2(H_2O)_2]^{8-}$ (X=S, Se, HP).[5a, 6] Colour scheme: orange: HP or Se or Te; yellow: S; indigo: W/Mo^{V}; grey: W; red: O.

$[Mo_2O_4(H_2O)_2]^{2+}$ was introduced as a reduced Mo source into the well-established synthetic system for pyramidal HA-templated POM cages (see SI for details).[11] Dark blue crystals $(C_2H_8N)_7H_3[W_{16}{}^{VI}Mo_2{}^{V}O_{54}(HPO_3)]\cdot 10H_2O$ (**1**), $(C_2H_8N)_7H_3[W_{16}{}^{VI}Mo_2{}^{V}O_{54}(SeO_3)]\cdot 10H_2O$ (**2**) and $(C_2H_8N)_7H_3[W_{16}{}^{VI}Mo_2{}^{V}O_{54}(TeO_3)]\cdot 10H_2O$ (**3**) were obtained from a reaction containing $Na_2WO_4\cdot 2H_2O$, dimethylamine hydrochloride (DMA·HCl), $[Mo_2O_4(H_2O)_2]^{2+}$ and $[XO_3]^{2-}$ (X=HP, Se, Te) at 50 °C. Single crystal X-ray structure analysis reveals that **1**-**3** share the same peanut-shaped framework of the previously reported single pyramidal HA-containing $\{W_{18}O_{54}(XO_3)\}$ (X = Bi, As, S)[5b,d,e], which consists of two equal $\{M_9O_{33}\}$ (M=W/Mo) moieties linked by six equatorial oxo ligands (Figure 1a and 1b), showing a distinct difference from the "Trojan horse"-type $[W_{18}O_{56}(XO_3)_2(H_2O)_2]^{8-}$ (Figure 1c).[6] Compared with these clusters, the novelty of compounds **1**-**3** arises from the reduced cage-like shell consisting of mixed Mo^{V}/W^{VI} metal sites, as confimed by their characteristic blue colour, derived from intervalence charge transfer between the mixed-valence metal sites, as well as by elemental analysis (see SI for details). In compounds **1**-**3**, HAs $[HPO_3]^{2-}$, $[SeO_3]^{2-}$ or $[TeO_3]^{2-}$ are enclosed in the half-cage $\{M_9O_{33}\}$ (M=W/Mo), respectively, and are displaced to occupy one side of the cluster, deviating ~1.27 Å from the centre (Figure 1a). A similar phenomenon has also been found in the reported $\{W_{18}O_{54}(XO_3)\}$ (X = Bi, As, etc.) analogues.

Under more dilute conditions, decreasing the ratio of $[WO_4]^{2-}/[XO_3]^{2-}$ led to the formation of three-layered cage structures $(C_2H_8N)_{11}Na_1H_1[W_{21}{}^{VI}Mo_3{}^{V}O_{75}(HPO_3)_2]\cdot 15H_2O$ (**4**), $(C_2H_8N)_{11}Na_1H_1[W_{21}{}^{VI}Mo_3{}^{V}O_{75}(SeO_3)_2]\cdot 15H_2O$ (**5**), and $(C_2H_8N)_{10}Na_1H_1[W_{22}{}^{VI}Mo_2{}^{V}O_{75}(TeO_3)_2]\cdot 15H_2O$ (**6**). Compound **4** can be regarded as a novel extended peanut-shaped cage, by effectively inserting an additional layer of $\{M_6(HPO_3)\}$ (M=W/Mo) into the middle of compound **1** (Figure 2). The two $[HPO_3]^{2-}$ heteroanions, located in the middle and top layers, display an eclipsed arrangement with respect to one another. Interestingly, in contrast to all known cylinder-shaped POM cage clusters, compound **5** and **6** are neither olive-shaped nor peanut-shaped, but an unprecedent bullet-shaped structure with a pointed top and flat bottom (Figure 2). Overall, the molecular structures of **5** and **6** can be considered as an integrated cluster built from $\{M_{15}(XO_3)_2\}$ (X=Se or Te) unit in an olive-shaped Dawson and $\{M_9\}$ unit in a peanut-shaped Dawson. Due to the size restriction within **5** and **6**, only two HAs are located on the two belts near the pointed end, in an eclipsed arrangement, leaving the belt near the bottom end empty. It should be noted that compounds **4**-**6** represent the first examples of three-layered cage-like POM clusters containing multiple HAs; the discovery of which greatly diversifies the structural library of Dawson-type clusters. More importantly, the presence of both olive-shaped and peanut-shaped Dawson fragments in one moiety (**5** and **6**) shows the potential to build novel multi-layered clusters based on controlled aggregation of these building blocks. Moreover, the formation of **5** and **6** under the same conditions as **4** implies the electronic nature and size of the HAs also play an important role in directing the assembly of the resultant clusters.

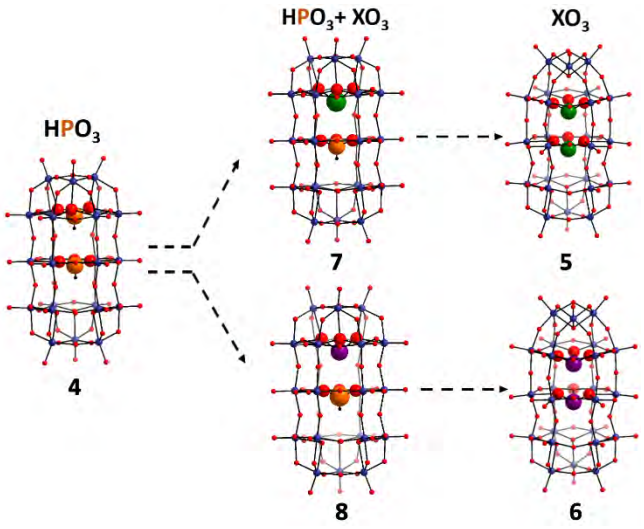

Figure 2. Structural representations of pyramidal heteroanions controlled assembly of extended three-layered peanut-shaped cages **4**, **7**, **8** and bullet-shaped cages **5** and **6**, where X=Se or Te. Colour scheme: orange: P; green: Se; purple: Te; indigo: W/Mo^{V}; red: O; black: hydrogen.

To further explore and understand the influence of HAs on the self-assembly of multi-layered POM clusters, mixed HAs of phosphite and selenite or phosphite and tellurite were introduced into the synthesis under the same reaction conditions of **4**-**6**, resulting in two three-layered analogues $(C_2H_8N)_{10}Na_1H_1[W_{22}{}^{VI}Mo_2{}^{V}O_{75}(HPO_3)(SeO_3)]\cdot 15H_2O$ (**7**) and $(C_2H_8N)_{11}Na_1H_1[W_{21}{}^{VI}Mo_3{}^{V}O_{75}(HPO_3)(TeO_3)]\cdot 15H_2O$ (**8**), respectively (Figure 2). Due to the distinctly different electronic properties and relative sizes between the two mixed HAs, they were completely differentiated and incorporated into two well-defined positions via self-sorting, a principle which has already been successfully applied in the assembly of cross-shaped POM clusters $[(XYW_{15}O_{54})_4(WO_2)_4]^{32-/36-}$ (X=HP, Y=Se, Te, As).[12] Structure determination reveals **7** and **8** share the same framework as **4**, in which $[HPO_3]^{2-}$ is always located at the centre

of the middle belt while the larger $[SeO_3]^{2-}$ or $[TeO_3]^{2-}$ are disordered equally at the two ends with half occupancies (Figure 2). This arrangement results from the approximately tetrahedral configuration adopted by $[HPO_3]^{2-}$, which requires more space for its accommodation compared with pyramidal-shaped $[SeO_3]^{2-}$ or $[TeO_3]^{2-}$, and thus preferentially occupies the middle of the structure while keeping one end occupied by another type of HA. The same arrangement has also been observed in the cross-shaped POM clusters where the smaller $[HPO_3]^{2-}$ occupies the uncapped end.[12] Based on the crystal structures of **4**-**8**, it can be concluded that the architectures of three-layered POM clusters are directly regulated by the selected HAs. The smaller $[HPO_3]^{2-}$ always favours the formation of extended peanut-like cages, even in the presence of another type of pyramidal HA, while larger $[XO_3]^{2-}$ (X=Se, Te) solely facilitates the assembly of bullet-shaped clusters.

Figure 3. Structural representations of $[HPO_3]^{2-}$ templated four-layered cage structure $[W_{26}{}^{VI}Mo_4{}^{V}O_{93}(HPO_3)_3]^{16-}$ (**9**) and $[SeO_3]^{2-}$ templated cluster **10** consisting of a four-layered $[W_{26}{}^{VI}Mo_4{}^{V}O_{93}(SeO_3)_3]^{16-}$ (**10a**) cocrystallized with a dimeric "Trojan-Horse" type cluster $[W_{36}O_{112}(SeO_3)_4]^{16-}$ (**10b**). Colour scheme: orange: HP; green: Se; indigo: W^{VI}/Mo^{V}; red: O; black: hydrogen.

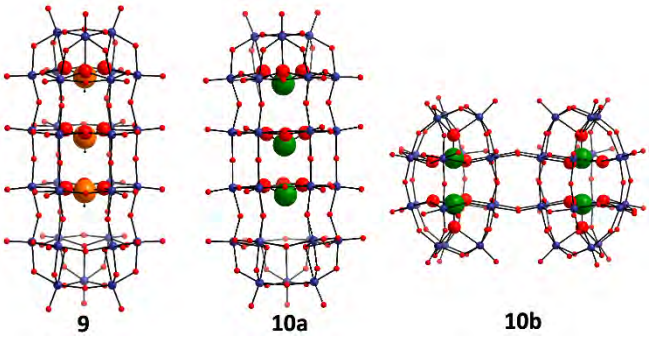

The successful isolation of a series of three-layered POM cages encouraged us to further extend multi-layered clusters. Under the same synthetic conditions of **4**, a slight increase of the temperature from 50 to 65 °C led to the generation of a four-layered cluster $(C_2H_8N)_{16}[W_{26}{}^{VI}Mo_4{}^{V}O_{93}(HPO_3)_3]\cdot 15H_2O$ (**9**) as a side product of **4**. Compund **9** also shows an extended peanut-shaped cage structure but with four belt layers capped by two $\{M_3\}$ (M=W/Mo) triads (Figure 3). In this context, the shell of **9** could be regarded as a fusion of lacunary $\{M_{15}O_{39}(HPO_3)_2\}$ and $\{M_{15}O_{39}(HPO_3)\}$ (M=W/Mo) moieties. In total there are three $[HPO_3]^{2-}$ encapsulated in **9**, which are evenly disordered on the consecutive three belts from either end. Although four-layered POM cages $\{M_{30}O_{90}(P_2O_7)_n(XO_3)_m\}$ (M =W, Mo; X = HP, Se; n = 1, 2; m = 2, 0) have been reported by adopting either pyrophosphate or a mixture of pyrophosphate and pyramidal $\{XO_3\}$ as templates,[7] we demonstrate here for the first time that four-layered cages can be constructed from a single type of $\{XO_3\}$, which not only represents a key step towards the versatile synthesis of $\{XO_3\}$-templated multi-layered clusters but also realizes our previous hypothesis to build four-layered HPOMs based on unconventional HAs.[13]

To our delight, replacing $[HPO_3]^{2-}$ with $[SeO_3]^{2-}$ in the synthesis afforded $(C_2H_8N)_{30}Na_1H_1[W_{26}{}^{VI}Mo_4{}^{V}O_{93}(SeO_3)_3][W_{36}{}^{VI}O_{112}(SeO_3)_4]\cdot 40H_2O$ (**10**) as the exclusive product. This cluster consists of a four-layered $[Se_3W_{26}Mo_4O_{102}]^{16-}$ (**10a**) cocrystallized with a dimeric cluster $[Se_4W_{36}O_{124}]^{16-}$ (**10b**). **10a** is isostructural to the cluster in **9** but with three $[SeO_3]^{2-}$ anions distributed over the three belt layers (Figure 3 and Figure S1). **10b** is observed for the first time and features a dimeric motif constructed from two "Trojan-Horse" $[W_{18}O_{56}(SeO_3)_2(H_2O)_2]^{8-}$ ($\{Se_2W_{18}\}$) clusters by sharing the four water ligands (Figure 3).[6b] The presence of both peanut-shaped and "Trojan-Horse" clusters in **10** indicate the competitive formation of these clusters during the self-assembly. Indeed, "Trojan-Horse" $\{Se_2W_{18}\}$ was the predominant product after the reaction and compound **10** can only be obtained after the formation of $\{Se_2W_{18}\}$. Upon removing the crystals of $\{Se_2W_{18}\}$ over several instances, dark blue **10** started to appear in the solution with relatively low yield.

All the compounds **1**-**10** display broad absorption bands at around 550 and 850 nm in the UV-Vis-NIR spectra due to heteronuclear transitions $Mo^{5+}\rightarrow W^{6+}$ (see Figure S2).[14] Since polyoxomolybdates are easier to be reduced and can preserve the reduced clusters in both solution and solid-phase in comparison with POTs, we considered that all the Mo sites retain the original valence of +5 from $[Mo_2O_4(H_2O)_2]^{2+}$ whereas all the W centers adopt +6 oxidation state. Also, redox titration futher confirmed the presence of 2-4 reduced electrons in **1**-**10**, which is consistent with the ICP-OES data (see SI). It is worth noting that the presence of reduced Mo species is essential to induce the formation of multi-layered clusters **4**-**10**. Control experiments showed that only tungsten-based "Trojan-Horse" or "peanut" type $\{W_{18}\}$ clusters formed when replacing $[Mo_2O_4(H_2O)_2]^{2+}$ with fully oxidised $[MoO_4]^{2-}$ in the synthesis of **4**-**10**. In contrast, addition of reducing agents such as hydrazine to the solution containing $[WO_4]^{2-}$ and $[MoO_4]^{2-}$ led to the isolation of multi-layered structures in a similar manner to $[Mo_2O_4(H_2O)_2]^{2+}$ (see details in SI). Mixing reducing agents with $[WO_4]^{2-}$ under the same conditions, however, did not afford the targeted clusters but "Trojan-Horse" or "peanut" type $\{W_{18}\}$. These results clearly illustrate the key role of reduced Mo species in directing the self-assembly of multi-layered POM clusters and support our assumption that all the reduced electrons are located on Mo centers**.**

Due to the similar chemical properties of Mo and W, Mo in principle can occupy the same metal sites on the shells of compound **1**-**10** together with W. Therefore, it is impossible to determine the exact sites of Mo and the ratio of Mo:W from crystal structures. The current ratio of Mo:W presented in the formulae is deduced from ICP-OES analysis, which is an average result representing a statistic combination of all the possible compositions of W and Mo in the structures, as is evidenced by ESI-MS analysis of **1**-**3** (see Figure S3-S5 and Tables S5–S7 for specific assignments).[15] In order to further confirm the variable composition of W and Mo in one cluster, cation exchange was performed to exchange all the dimethylammonium in compound **3** with tetrabutylammonium (TBA), resulting in the isolation of fully oxidized $(C_{16}H_{36}N)_5[H_3TeW^{VI}{}_{16}Mo^{VI}{}_2]$ (**11**). In general, the TBA exchanged analogue will exhibit better MS response in organic phase than the pristine cluster in water. Additionally, it is difficult to obtain NMR signals with high resolution when the cluster is reduced and therefore the oxidized **11** is a good candidate for NMR study. As seen in the ESI-MS spectrum of compound **11** (Figure S6), intact molecular species was observed in charges ranging from -

5 to -3 with different compositions varying from $\{W_{17}Mo_1(TeO_3)\}$ to $\{W_{13}Mo_5(TeO_3)\}$ (see Table S8). This is further verified by NMR studies. As shown in Figure S7, ^{125}Te NMR spectrum of compound **11** exhibits multiple peaks in the region of 1769-1779 ppm. The presence of multiple peaks with similar chemical shifts indicates that a mixture of $\{W_{18-x}Mo_x(TeO_3)\}$ clusters with varying Mo/W compositions coexist in the solution, as only one singlet should be observed for a pure cluster with specific composition, which is the case of cross-shaped $[W_{64}O_{220}(HPO_3)_4(TeO_3)_4]^{32-}$.[12]

A salt mixed-valence Keggin $[PMo^{V}_2Mo^{VI}_{10}O_{40}]^{5-}$ was reported to exhibit dielectric relaxation around 50-120 K that was correlated to the mixed-valence system.[16] Temperature dependent dielectric properties of compounds **3**, **4** and **6** (measured using pellets) showed similar Debye-type relaxation at 50-150 K (Figure 4 and Figure S8-S9). According to Arrhenius equations with temperature and frequency for a peak of ε_2, activation energies of relaxation were estimated to be 0.13, 0.15 and 0.10 eV for **3**, **4** and **6**, respectively. These values are relatively lower than that expected for proton conduction by crystalline water.[17] Thermal motion by cation also requires higher activation energy than proton hopping. An ε_1 value reached 10^1-10^2 upon heating to room temperature. Such a large value is indicative of enriched thermal motion of cations and proton conduction. It was deduced that rapid dipole relaxations observed around 50-150 K is due to the mixed-valence system in the multi-layered POM cages, demonstrating their potential use for electronic devices.

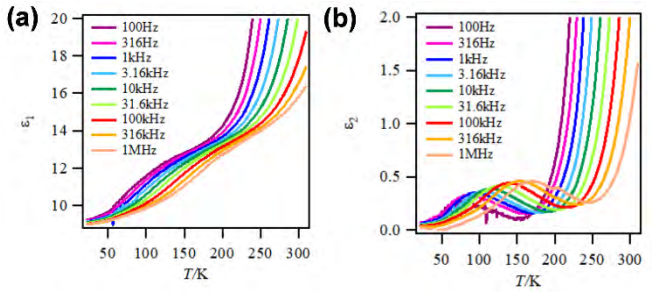

Figure 4. Temperature dependence of a) real ε_1 and b) imaginary ε_2 parts of the complex dielectric constant for **3**, characterized by the impedance method in the frequency range from 100 Hz to 1 MHz and were plotted.

In summary, we describe the heteroanion-directed and reduction-driven assembly of a series of multi-layered POM cages **1**-**10** templated by 1-3 redox-active pyramidal HAs. Compound **1**-**3** share the same two-layered peanut-shaped framework of $\{W_{18}O_{54}(XO_3)\}$ templated by one HA. Under more diluted conditions, decreasing the ratio of $[WO_4]^{2-}/[XO_3]^{2-}$ led to the formation of three-layered cage structures **4**-**8** that feature either unprecedent extended peanut-shape or bullet-shaped cage structures, regulated by the HAs. This not only renews the structural library of Dawson-type clusters but also emphasizes the key role of HAs in the self-assembly. Slight increase of the reaction temperature led to the generation of four-layered clusters **9** and **10**, which show four-layered cage structures similar to the reported $\{M_{30}O_{90}\}$ but solely constructed from three pyramidal HAs. Control experiments indicated reduced Mo is essential for the self-assembly of multi-layered POM cages **4**-**10**, and the presence of reduced Mo^{V} and variable compositions of W and Mo in **1**-**10** were confirmed by UV-Vis-NIR, NMR spectroscopy and mass spectrometry. Moreover, the ESI-MS and NMR study of fully oxidized **11** further confirmed the variable composition of W and Mo in **1**-**10**. Due to the presence of reduced Mo^{V} centers, dipole relaxations in the multi-layered POM cages were observed, demonstrating their potential use for electronic devices. In the future, we will further extend the utility of reduced Mo species in directing the self-assembly of redox-active POM clusters bearing more than four layers and explore their potential applications in electronic materials.

Acknowledgements

This work was supported by the EPSRC grants (No. EP/J015156/1; EP/L023652/1; EP/I033459/1; EP/J015156/1; EP/K023004/1; EP/L023652/1), EC grant 318671 MICREAGENTS, LC thanks the Royal Society / Wolfson Foundation for a Merit Award and the ERC for an Advanced Grant (ERC-ADG, 670467 SMART-POM). We thank the Diamond Light Source for time on Beamline I19 under the proposal MT16085. We would also like to thank A. Bubliauskas and E. Nicholson of University of Glasgow for assistance with compound synthesis and analysis.

Keywords: self-assembly • polyoxometalates • reduction-driven • cage compound

[1] a) C. Yuan, H. Bin Wu, Y. Xie, X. W. Lou, *Angew. Chem.* **2014**, 126, 1512-1530; *Angew. Chem. Int. Ed.* **2014**, *53*, 1488-1504; b) J. Suntivich, H. A. Gasteiger, N. Yabuuchi, H. Nakanishi, J. B. Goodenough, Y. Shao-Horn, *Nat. Chem.* **2011**, *3*, 546-550; c) X. Yu, T. J. Marks, A. Facchetti, *Nature Mater.* **2016**, *15*, 383-396.

[2] a) D. L. Long, R. Tsunashima, L. Cronin, *Angew. Chem*. **2010**, *122*, 1780 – 1803; *Angew. Chem. Int. Ed.* **2010**, *49*, 1736-1758; b) Y. F. Song, R. Tsunashima, *Chem. Soc. Rev.* **2012**, *41*, 7384–7402; c) N. Mizuno, M. Misono, *Chem. Rev.* **1998**, *98*, 199–217; d) E. Coronado, C. J. Gómez-García, *Chem. Rev.* **1998**, *98*, 273–296.

[3] a) M. T. Pope, *Heteropoly and Isopolyoxometalates*, Springer-Verlag Berlin Heidelberg, **1983**; b) A. Banerjee, B. S. Bassil, G. V. Röschenthaler, U. Kortz, *Chem. Soc. Rev.* **2012**, *41*, 7590–7604; c) J. J. Chen, M. D. Symes, L. Cronin, *Nat. Chem.* **2018**, *10*, 1042–1047.

[4] a) C. Fleming, D.-L. Long, N. McMillan, J. Johnston, N. Bovet, V. Dhanak, N. Gadegaard, P. Kögerler, L. Cronin, M. Kadodwala, *Nat. Nanotechnol.* **2008**, *3*, 289–233; b) D. L. Long, P. Kögerler, L. Cronin, *Angew. Chem*. **2004**, *116*, 1853-1856; *Angew. Chem. Int. Ed.* **2004**, *43*, 1817-1820.

[5] a) D. L. Long, H. Abbas, P. Kögerler, L. Cronin, Angew. Chem. **2005**, *117*, 3481-3485; *Angew. Chem. Int. Ed.* **2005**, *44*, 3415-3419; b) Jun Yan, De-Liang Long, N. M. Haralampos, L. Cronin, *Inorg. Chem.* **2010**, *49*, 1819–1825; c) L. Wang, W. Li, L. Wu, X. Dong, H. Hu, G.-L. Xue, *Inorg. Chem. Commun.* **2013**, *35*, 122–125; d) Y. Jeannin, J. Martin-Frère, *Inorg. Chem.* **1979**, *18*, 3010–3014; e) Y. Ozawa, Y. Sasaki, *Chem. Lett.* **1987**, *16*, 923–926;

[6] a) Q. Zheng, L. Vilà-Nadal, C. Busche, J. S. Mathieson, D.-L. Long, L. Cronin, *Angew. Chemie* **2015**, *127*, 8006-8010; *Angew. Chem. Int. Ed.* ***2015***, *54*, 7895-7899; b) C. Busche, L. Vilà-Nadal, J. Yan, H. N. Miras, D.-L. Long, V. P. Georgiev, A. Asenov, R. H. Pedersen, N. Gadegaard, M. M. Mirza, D. J. Paul, J. M. Poblet, L. Cronin, *Nature* **2014**, *515*, 545-549.

[7] a) Maeda, T. Goto, M. Takamoto, E. Kazuo, S. Himeno, H. Takahashi, T. Hori, *Inorg. Chem.* **2008**, *47*, 11197-11201; b) K. Eda, K. Den, S. Himeno, *Inorg. Chim. Acta* **2012**, *382*, 182-185; c) U. Kortz, B. Street, P. O. Box, R. V June, *Inorg. Chem.* **2000**, *39*, 623-624; d) K. Eda, S.

Maeda, S. Himeno, T. Hori, *Polyhedron* **2009**, *28*, 4032-4038.

[8] a) A. Müller, P. Gouzerh, *Chem. Soc. Rev.* **2012**, *41*, 7431-7463; b) A. Müller, E. Krickemeyer, J. Meyer, H. Bögge, F. Peters, W. Plass, E. Diemann, S. Dillinger, F. Nonnenbruch, M. Randerath, C. Menke, *Angew. Chem.* **1995**, *107*, 2293-2295; *Angew. Chem. Int. Ed.* **1995**, *34*, 2122‑2124; c) A. Müller, E. Krickemeyer, H. Bögge, M. Schmidtmann, C. Beugholt, P. Kögerler, C. Lu, *Angew. Chem*. **1998**, *110*, 1278-1281; *Angew. Chem. Int. Ed*. **1998**, 37, 1220-1223; d) A. Müller, E. Beckmann, H. Bögge, M. Schmidtmann, A. Dress, *Angew. Chem*. **2002**, *114*, 1210-1215; *Angew. Chem. Int. Ed*. **2002**, *41*, 1162-1167.

[9] a) A. Müller, P. Kögerler, C. Kuhlmann, *Chem. Commun*. **1999**, 1347-1358; b) A. Müller, E. Krickemeyer, H. Bögge, M. Schmidtmann, F. Peters, *Angew. Chem*. **1998**, *110*, 3567-3571; *Angew. Chem. Int. Ed*. **1998**, *37*, 3359-3363.

[10] a) C. Schäffer, A. Merca, H. Bögge, A. M. Todea, M. L. Kistler, T. Liu, R. Thouvenot, P. Gouzerh, A. Müller, *Angew. Chem*. **2009**, *121*, 155-159; *Angew. Chem. Int. Ed.* **2009**, *48*, 149-153; b) C.Schaffer, A. M. Todea, H. Bögge, O. A. Petina, D. Rehder, E. T. K. Haupt, A. Müller, *Chem. Eur. J.* **2011**, *17*, 9634−9639.

[11] A. Dolbecq, J. D. Compain, P. Mialane, J. Marrot, F. Sécheresse, B. Keita, L. R. B. Holzle, F. Miserque, L. Nadjo, *Chem. Eur. J.* **2009**, *15*, 733-741.

[12] Q. Zheng, L. Vilà-Nadal, Z. Lang, J.-J. Chen, D.-L. Long, J. S. Mathieson, J. M. Poblet, L. Cronin, *J. Am. Chem. Soc*. **2018**, *140*, 2595-2601.

[13] J. Gao, J. Yan, S. Beeg, D.-L. Long, L. Cronin, *Angew. Chem*. **2012**,124, 3429 -3432; *Angew. Chem. Int. Ed.* **2012**, *51*, 3373-3376.

[14] a) L. V. Potapova, T. A. Karpukhina, L. P. Kazanaskii, V. I. Spitsyn. *Russ. Chem. Bull.* **1979**, 28, 674-678; b) H. So, M. T. Pope, *Inorg. Chem*. **1972**, *11*, 1441-1443.

[15] M. M. Sabi, J. Soriano-Lopez, R. S. Winter, J. -J. Chen, L. Vilà-Nadal, D. -L. Long, J. R. Galan-Mascaros, L. Cronin, *Nat. Cat.* **2018**, *1*, 208-213.

[16] I. Nakamura, R. Tsunashima, S. Nishihara, K. Inoue, T. Akutagawa, *Chem. Comm.* **2017**, *53*, 6824-6827.

[17] X. Meng, H.-N. Wang, S.-Y. Song, H.-J. Zhang, *Chem. Soc. Rev.* **2017**, *46*, 464-480.

Pyramidal Heteroanion-directed and Reduced Mo^{V}-driven assembly of Multi-layered Polyoxometalate Cages

Qi Zheng,[a] Manuel Kupper,[a] Weimin Xuan,[a] Hirofumi Oki,[b] Ryo Tsunashima,[b] De-Liang Long[a] and Leroy Cronin[a]

Abstract: The fabrication of redox-active polyoxometalates (POMs) that can switch between multiple states is critical for their application in electronic devices, yet, a sophisticated synthetic methodology is not well developed for such cluster types. Here we describe the heteroanion-directed and reduction-driven assembly of a series of multi-layered POM cages **1**-**10** templated by 1-3 redox-active pyramidal heteroanions. The heteroanions greatly affect the self-assembly of the resultant POM cages, leading to the generation of unprecedented three-layered peanut-shaped - **4**, **7** and **8** - or bullet-shaped - **5** and **6** - structures. The introduction of reduced molybdate is essential for the self-assembly of the compounds and results in mixed-metal (W/Mo), and mixed-valence (W^{VI}/Mo^{V}) **1**-**10**, as confirmed by redox titration, UV-Vis-NIR, NMR spectroscopy and mass spectrometry. **11**, the tetrabutyl ammonium (TBA) salt derivative of the fully oxidized **3**, is produced as a model structure for measurements to confirm that **1**-**10** are a statistical mixture of isostructural clusters with different ratios of W/Mo. Finally, multi-layered POM cages exhibit dipole relaxations due to the presence of mixed valence W^{VI}/Mo^{V} metal centers, demonstrating their potential uses for electronic materials.

Table of Contents

1. Materials and instrumentation

Materials.
Reagent-grade chemicals were obtained from Aldrich Chemical Company Ltd. and Alfa Aesar, and used without further purification.

Instrumentation.
Single Crystal X-ray Diffraction: Suitable single crystals were selected and mounted by using the MiTeGen MicroMountsTM kit with Fomblin oil. X-ray diffraction intensity data were measured at 150(2) K on Bruker Apex II Quasar diffractometers using Mo Kα [λ = 0.71073 Å]. Structure solution and refinement were carried out with SHELXS[1] and SHELXL-2014[2] via WinGX[3]. Corrections for incident and diffracted beam absorption effects were applied using empirical methods[4]. The X-ray crystallographic data for structures reported in this article have been deposited at the Cambridge Crystallographic Data Centre, under deposition number CCDC-1885487-1885496. These data can be obtained free of charge via www.ccdc.cam.ac.uk/data_request/cif, or by emailing

data_request@ccdc.cam.ac.uk, or by contacting The Cambridge Crystallographic Data Centre, 12 Union Road, Cambridge CB2 1EZ, UK; fax: +44 1223 336033.

UV-Vis-NIR spectroscopy: UV-Vis-NIR spectroscopy experiments were carried out using a SPECORD S600 Analytic Jena spectrophotometer. The measurements were performed in a quartz glass cuvette with optical path length 2.0 mm.

Microanalysis: Carbon, nitrogen and hydrogen content were determined by the microanalysis services within the Department of Chemistry, University of Glasgow using an EA 1110 CHNS, CE-440 Elemental Analyzer.

Inductively Coupled Plasma Optical Emission Spectroscopy (ICP-OES): Samples were prepared in 3 mL HNO_3/ 2 mL H_2O_2 and diluted with water to make 50 mL total volume. The relative error in the measurements is ± 3%.

Fourier-transform infrared (FT-IR) spectroscopy: The sample was prepared as a KBr pellet and the FT IR spectrum was collected in transmission mode in the range of 400-4000 cm^{-1} using a JASCO FT-IR 4100 spectrometer. Wavenumbers are given in cm^{-1}.

Thermogravimetric Analysis (TGA): Thermogravimetric analysis was performed on a TA Instruments Q 500 Thermogravimetric Analyzer under nitrogen flow at a typical heating rate of 10°C min^{-1}.

Redox titration: Redox titration of the compounds was performed by using cerium ammonium nitrate (0.0025 M) in 0.5 M H_2SO_4 as the oxidant.

Electrospray-ionization mass spectrometry (ESI-MS): All MS data was collected using a Q-trap, time-of-flight MS (Maxis Impact) instrument supplied by Bruker Daltonics Ltd. A Bruker Ltd cryospray source was used to collect data under the conditions specified below. The detector was a time-of-flight, micro-channel plate detector and all data was processed using the BrukerDaltonics Data Analysis 4.1 software, whilst simulated isotope patterns were investigated using Bruker Isotope Pattern software and Molecular Weight Calculator 6.45. All peak assignments were made *via* comparison of the experimentally determined isotopic patterns for each peak with simulated isotopic patterns. The sample solutions of **1**-**3** were prepared by dissolving the compounds in a water/ acetonitrile (5 %:95 %) mixture (1 mg mL^{-1}) and sample solution of **11** was prepared by dissolving the compounds in acetonitrile 1 mg mL^{-1}.

Nuclear Magnetic Resonance Spectroscopy: ^{125}Te NMR spectroscopy were recorded on Bruker AVIII 600MHz spectrometer.

Dielectric measurement: Temperature-dependent dielectric permittivity was measured using an Agilent E4980A Precision LCR meter between 100 and 310 K controlled at 0.5 K/min. The pellets were made from a powdered sample after drying. The typical applied AC voltage was 1 V, and the frequency range was 100 Hz – 1 MHz.

2. Synthetic procedure:

Synthesis of $[Mo^{V}_2O_4(H_2O)_2]^{2+}$ in 4 M HCl ({Mo_2})

The synthesis is based on reported procedure.[5] 840 µL of hydrazine monohydrate (64-65 %) was added to a suspension of 9.2 g molybdenum trioxide in 320 mL 4 M HCl. The solution was heated at 60°C for 3 hours.

Synthesis of $(C_2H_8N)_7H_3[HPW_{16}Mo_2O_{60}]\cdot 10H_2O$ (1)

Sodium tungstate dihydrate (2.5 g, 7.6 mmol), phosphorous acid (0.04 g, 0.48 mmol) and dimethylamine hydrochloride (DMA·HCl) (1.2 g, 14.7 mmol) were dissolved in 20 mL water. Around 2.8 mL of {Mo_2} was added dropwise under stirring, and the solution pH consequently reached 2.2. The solution was heated with stirring at around 50 °C for 30 mins. Cool down to room temperature, dark blue powder formed and was removed by filtration. Dark blue block crystals were isolated from the filtrate after a few days. These crystals were collected by soaking the solid using filtered mother liquid to remove further blue powder (Yield: 8.3% based on W).

Characteristic IR bands (cm^{-1}): 3419(b), 3151(b), 2980(s), 2785(w), 2451(w), 1614(m), 1462(s), 1379(m), 1249(w), 1153(w), 1066(m), 951(s), 721(s), 501(w). Elemental Analysis for $C_{14}H_{80}N_7P_1W_{16}Mo_2O_{70}$, M_W = 4631.23 g mol^{-1}, calc (%): W 63.51, Mo 4.14, P 0.67, H 1.74, C 3.63, N 2.11; found (%): W 64.09, Mo 3.87, P 0.76, H 1.63, C 3.14, N 2.32. Calculated TGA water loss from 25 to 200 °C (%) calculated: 3.9, found 3.1.

Synthesis of $(C_2H_8N)_7[H_3SeW_{16}Mo_2O_{60}]\cdot 10H_2O$ (2)

Sodium tungstate dihydrate (2.5 g, 7.6 mmol), sodium selenite (0.08 g, 0.46 mmol) and dimethylamine hydrochloride (DMA·HCl) (1.2 g, 14.7 mmol) were dissolved in 20 mL water. 2.8-3.4 mL of $\{Mo_2\}$ was added dropwise under stirring, and the solution pH consequently reached 1.3-2.6. The solution was heated with stirring at around 50 °C for 30 mins. Cool down to room temperature, dark blue powder formed and was removed by filtration. Dark blue block crystals were isolated from the filtrate after one week. These crystals were collected by soaking the solid using filtered mother liquid to remove further blue powder (Yield: 22.4% based on W). Characteristic IR bands (cm^{-1}): 3452(b), 3140(b), 2980(s), 2779(m), 2453(w), 1614(m), 1462(s), 1388(m), 1253(w), 1161(s), 1068(m), 1018(m), 950(s), 704(s). Elemental Analysis for $C_{14}H_{79}N_7Se_1W_{16}Mo_2O_{70}$, M_W = 4678.21 g mol^{-1}, calc (%): W 62.87, Mo 4.10, Se 1.68, H 1.70, C 3.59, N 2.09; found (%): W 57.36, Mo 3.19, Se 1.77, H 1.56, C 3.53, N 2.03. Calculated TGA water loss from 25 to 200 °C (%) calculated: 3.8, found 3.3.

Synthesis of $(C_2H_8N)_7[H_3TeW_{16}Mo_2O_{60}]\cdot 10H_2O$ (3)

Sodium tungstate dihydrate (2.5 g, 7.6 mmol), sodium tellurite (0.1 g, 0.48 mmol) and dimethylamine hydrochloride (DMA·HCl) (1.2 g, 14.7 mmol) were dissolved in 20 mL water. Around 3 mL of $\{Mo_2\}$ was added dropwise under stirring, and the solution pH consequently reached 1.9. The solution was heated with stirring at around 50 °C for 30 mins. Cool down to room temperature, big dark blue block crystals were isolated from the filtrate after one week. (Yield: 62.5 % based on W). Characteristic IR bands (cm^{-1}): 3448(b), 3159(b), 3035(b), 2786(m), 2447(w), 1614(m), 1463(s), 1244(w), 1071(m), 957(s), 877(s), 713(s), 487(w). Elemental Analysis for $C_{14}H_{79}N_7Te_1W_{16}Mo_2O_{70}$, M_W = 4726.85 g mol^{-1}, calc (%): W 62.23, Mo 4.06, Te 2.70, H 1.68, C 3.56, N 2.07; found (%): W 61.87, Mo 4.28, Te 2.76, H 1.77, C 3.93, N 2.26. Calculated TGA water loss from 25 to 200 °C (%) calculated: 3.8, found 1.8.

Synthesis of $(C_2H_8N)_{11}Na_1[H_3P_2W_{21}Mo_3O_{81}]\cdot 15H_2O$ (4)

Sodium tungstate dihydrate (1.6 g, 4.8 mmol), phosphorous acid (0.04 g, 0.48 mmol) and dimethylamine hydrochloride (DMA·HCl) (1.2 g, 14.7 mmol) were dissolved in 40 mL water. Around 1.6 mL of $\{Mo_2\}$ was added dropwise under stirring, and the solution pH consequently reached 3.3. The solution was heated with stirring at around 50 °C for 30 mins. Cool down to room temperature, dark blue powder formed and was removed by filtration. Dark blue precipitates appear after a few days and were removed by filtration. Small dark blue star or rod-like crystals were isolated after three weeks. These crystals were collected by soaking the solid using filtered mother liquid to remove further blue powder (Yield: 6.3% based on W). Characteristic IR bands (cm^{-1}): 3448(b), 3140(b), 2980(s), 2787(w), 2455(w), 1614(m), 1462(s), 1381(m), 1251(m), 1149(s), 1066(m), 952(s), 731(s). Elemental Analysis for $C_{22}H_{121}N_{11}Na_1P_2W_{21}Mo_3O_{96}$, M_W = 6309.8 g mol^{-1}, calc (%): W 61.19, Mo 4.56, P 0.98, Na 0.36, H 1.93, C 4.19, N 2.44; found (%): W 59.66, Mo 4.24, P 0.76, Na 0.79, H 1.80, C 4.06, N 2.33. Calculated TGA water loss from 25 to 200 °C (%) calculated: 4.3, found 2.8.

Synthesis of $(C_2H_8N)_{11}Na_1[H_1Se_2W_{21}Mo_3O_{81}]\cdot 15H_2O$ (5)

Sodium tungstate dihydrate (1.36 g, 4.1 mmol), sodium selenite (0.08 g, 0.46 mmol) and dimethylamine hydrochloride (DMA·HCl) (1.2 g, 14.7 mmol) were dissolved in 20 mL water. Around 1.5 mL of $\{Mo_2\}$ was added dropwise under stirring, and consequently the solution pH reached 2.2. The solution was heated with stirring at around 50 °C for 30 mins. Cool down to room temperature, dark blue powder formed and was removed by filtration. Blue precipitates appear constantly, and were removed by filtration. Small dark blue needle-shaped crystals were isolated from the filtrate after three months. These crystals were collected by soaking the solid using filtered mother liquid to remove further blue powder (Yield: 8.0% based on W). Characteristic IR bands (cm^{-1}): 3431(b), 3159(b), 2980(m), 2879(w), 2786(w), 2436(w), 1614(m), 1462(m), 1379(m), 1253(m), 1153(m), 1070(m), 952(s), 746(s), 488(w). Elemental Analysis for $C_{22}H_{119}N_{11}Na_1Se_2W_{21}Mo_3O_{96}$, M_W = 6403.75 g mol^{-1}, calc (%): W 60.29, Mo 4.49, Se 2.47, Na 0.36, H 1.87, C 4.12, N 2.41; found (%): W 61.87, Mo 4.48, Se 1.90, Na 0.34, H 1.71, C 4.60, N 2.40. Calculated TGA water loss from 25 to 200 °C (%) calculated: 4.2, found 3.2.

Synthesis of $(C_2H_8N)_{10}Na_1[H_1Te_2W_{22}Mo_2O_{81}]\cdot 15H_2O$ (6)

Sodium tungstate dihydrate (7.5 g, 22.75 mmol), sodium tellurite (0.3 g, 1.35 mmol) and dimethylamine hydrochloride (DMA·HCl) (3.6 g, 44.1 mmol) were dissolved in 80 mL water. Around 9.2 mL of $\{Mo_2\}$ was added dropwise under stirring, and consequently, the solution pH reached 2.5. The solution was heated with stirring at around 50 °C for 30 mins. Cool down to room temperature, dark blue powder formed and was removed by filtration. Compound **3** formed and were isolated after a few days. Afterwards, blue precipitates appear constantly, and were removed by filtration. Finally, small dark blue rod-like crystals were isolated from the filtrate after four months. These crystals were collected by soaking the solid using filtered mother liquid to remove further blue powder (Yield: 7.5% based on W). Characteristic IR bands (cm^{-1}): 3444(b), 3143(b), 2981(m), 2783(w), 2443(w), 1608(m), 1463(s), 1382(w), 1247(w), 155(w), 1082(m), 1014(m), 954(s), 858(w), 725(s), 472(w). Elemental Analysis for $C_{20}H_{111}N_{10}Na_1Te_2W_{22}Mo_2O_{96}$, M_W = 6452.78 g mol^{-1}, calc (%): W 61.81, Mo 2.93, Te 3.90, Na 0.35, H 1.71, C 3.67, N 2.14; found (%): W 62.73, Mo 3.49, Te 4.82, Na 0.60, H 1.62, C 4.14, N 2.50. Calculated TGA water loss from 25 to 200 °C (%) calculated: 4.1, found 2.5.

Synthesis of $(C_2H_8N)_{10}Na_1H_1[HSePW_{22}Mo_2O_{81}]\cdot 15H_2O$ (7)

Sodium tungstate dihydrate (2.5 g, 7.6 mmol), phosphorous acid (0.02 g, 0.24 mmol), sodium selenite (0.04 g, 0.23 mmol) and dimethylamine hydrochloride (DMA·HCl) (1.2 g, 14.7 mmol) were dissolved in 20 mL water. Around 2.6 ml of $\{Mo_2\}$ was added

dropwise under stirring, and the solution pH consequently reached 2.0. The solution was heated with stirring at around 50°C for 30 mins. Cool down to room temperature, dark blue powder formed and was removed by filtration. Peanut-shaped clusters formed after a few weeks and were removed from the solution by filtration. Blue precipitates appear constantly afterward and were also removed by filtration. After two months, blue block crystals of **7** were formed and isolated. These crystals were collected by soaking the solid using filtered mother liquid to remove further blue powder (Yield:13.0% based on P or Se). Characteristic IR bands (cm^{-1}): 3430(b), 3032(b), 2758(w), 1694(m), 1464(s), 1246(w), 1064(m), 1016(m), 957(s), 892(w), 722(s), 550(w). Elemental Analysis for $C_{20}H_{112}N_{10}Na_1Se_1P_1W_{22}Mo_2O_{96}$, M_W = 6398.59 g mol^{-1}, calc (%): W 63.21, Mo 3.00, P 0.48, Se 1.23, Na 0.36, H 1.76, C 3.75, N 2.19; found (%): W 59.12, Mo 3.63, P 0.87, Se 1.54, Na 0.25, H 1.75, C 3.87 N 2.20. Calculated TGA water loss from 25 to 200°C (%) calculated: 4.2, found 4.1.

Synthesis of $(C_2H_8N)_{11}Na_1H_1[HTePW_{21}Mo_3O_{81}]\cdot 15H_2O$ (8)

Sodium tungstate dihydrate (2.5 g, 7.6 mmol), phosphorous acid (0.02 g, 0.24 mmol), sodium tellurite (0.05 g, 0.24 mmol) and dimethylamine hydrochloride (DMA·HCl) (1.2 g, 14.7 mmol) were dissolved in 20 mL water. Around 2.4 mL of $\{Mo_2\}$ was added dropwise under stirring, and the solution pH consequently reached 3.3. The solution was heated with stirring at around 50 °C for 30 mins. Cool down to room temperature, dark blue powder formed and was removed by filtration. Peanut-shaped clusters formed after a few weeks and were removed from the solution by filtration. Blue precipitates appear constantly afterwards and were also removed by filtration. Dark blue block crystals were isolated from the filtrate after six weeks. These crystals were collected by soaking the solid using filtered mother liquid to remove further blue powder (Yield: 20.0 % based on P). Characteristic IR bands (cm^{-1}): 3448(b), 2958(w), 3035(b), 2872(w), 2764(m), 2420(w), 1596(m), 1463(s), 1410(w), 1379(w), 1067(m), 1016(m), 958(s), 884(s), 736(s), 563(w). Elemental Analysis for $C_{20}H_{102}N_{10}Na_1P_1Te_1W_{21}Mo_3O_{91}$, M_W = 6269.25 g mol^{-1}, calc (%): W 61.58, Mo 4.59, P 0.49, Te 2.04, Na 0.37, H 1.64, C 3.83, N 2.23; found (%): W 55.1, Mo 4.19, P 0.64, Te 2.5, Na 0.29, H 1.57, C 3.70, N 2.10. Calculated TGA water loss from 25 to 200 °C (%) calculated: 4.3, found 2.6.

Synthesis of $(C_2H_8N)_{16}[H_3P_3W_{26}Mo_4O_{102}]\cdot 15H_2O$ (9)

Sodium tungstate dihydrate (1.6 g, 4.8 mmol), phosphorous acid (0.04 g, 0.48 mmol) and dimethylamine hydrochloride (DMA·HCl) (1.2 g, 14.7 mmol) were dissolved in 40 mL water. Around 1.6 ml of $\{Mo_2\}$ was added dropwise under stirring, and the solution pH consequently reached 3.2. The solution was heated with stirring at around 65 °C for 30 mins. Cool down to room temperature, dark blue powder formed and was removed by filtration. Blue precipitates appear constantly afterwards and were also removed by filtration. Dark blue bar-shaped crystals of **9** mixed with **4** were found from the filtrate after two months.

Synthesis of $(C_2H_8N)_{30}Na_1H_1[Se_3W_{26}Mo_4O_{102}][Se_4W_{36}O_{124}]\cdot 40H_2O$ (10)

Sodium tungstate dihydrate (1.6 g, 4.8 mmol), sodium selenite (0.08 g, 0.46 mmol) and dimethylamine hydrochloride (DMA·HCl) (1.2 g, 14.7 mmol) were dissolved in 40 mL water. Around 2.1 mL of $\{Mo_2\}$ was added dropwise under stirring, and consequently the solution pH reached 2.4. The solution was heated with stirring at around 65 °C for 30 mins. Cool down to room temperature, dark blue powder formed and was removed by filtration. Precipitates formed constantly and were removed by filtration. Then, pale blue precipitates together with "Trojan Horse"-type $[Se_2W_{18}O_{62}(H_2O)_2]^{8-}$[6] appear. Dark blue needle-shaped crystals of **10** were isolated from the filtrate after two months. These crystals were collected by soaking the solid using filtered mother liquid to remove further blue powder (Yield: 11.4% based on Se). Characteristic IR bands (cm^{-1}): 3455(b), 3137(b), 2786(w), 1605(m), 1464(m), 1016(m), 951(s), 714(s), 646(s). Elemental Analysis for $C_{60}H_{331}N_{30}Na_1Se_7W_{62}Mo_4O_{271}$, M_W = 18077.8 g mol^{-1}, calc (%): W 63.05, Mo 2.12, Se 3.06, Na 0.12, H 1.78, C 3.99, N 2.32; found (%): W 58.89, Mo 2.13, Se 3.31, Na 0.17, H 1.62, C 4.15, N 2.30. Calculated TGA water loss from 25 to 200°C (%) calculated: 4.0, found 3.7.

Synthesis of $(C_{16}H_{36}N)_5[H_3TeW_{16}Mo_2O_{60}]$ (11)

2.0 g of compound **3** (0.42 mmol) was dissolved in 25 mL of 0.5 M HCl. Then 15 mL solution of 5.0 g of tetrabutylammonium bromide was added under vigorous stirring. Blue powder was formed and isolated by centrifugation and collected, washed with water, ethanol and then dried under vacuum. Recrystallization of the solid from acetonitrile with ether diffusion afforded yellow crystals of **11.** (Yield: 37.10% based on compound **3**). Characteristic IR bands (cm^{-1}): 2958(m), 2872(m), 1482(s), 1464(m), 1378(m), 1151(w), 967(s), 951(s), 888(s), 771(s), 738(s). Elemental Analysis for $C_{80}H_{183}N_5Te_1W_{16}Mo_2O_{60}$, M_W = 5436.4 g mol^{-1}, calc (%): W 54.10, Mo 3.53, Te 2.35, H 3.39, C 17.67, N 1.29; found (%): W 54.50, Mo 3.15, Te 3.50, H 3.34, C 17.83, N 1.30. Calculated TGA solvent loss from 25 to 250 °C (%) calculated: 0.0, found 1.0.

Control Experiments:

The synthesis of **4** was chosen as a synthetic control experiment, following the general procedure:

Sodium tungstate dihydrate (1.6 g, 4.8 mmol), phosphorous acid (0.04 g, 0.48 mmol) and dimethylamine hydrochloride (DMA·HCl) (1.2 g, 14.7 mmol) were dissolved in 40 mL water. Sodium molybdate dihydrate (0.04 g, 0.16 mmol) was added to the solution. Then, 10 µL of hydrazine hydrate (64-65 %) was added to the solution dropwise, followed by adjusting the pH to 2.40 by 12 M HCl. The solution was heated with stirring at around 50 °C for 30 mins. Upon cooling down to room temperature, dark blue powder formed and was removed by filtration. The dark blue precipitates appeared after a few days and were removed by filtration again. Small dark blue rod-like crystals of **4** were isolated after one month. Alternatively, sodium molybdate dihydrate and hydrazine hydrate can be replaced by molybdenum(V) chloride (0.1 g, 0.37 mmol) under the same conditions with pH ranging from 2.5 to 3.4, which led to the formation of compound **4** as well. Note that the original synthesis of **4** involves $[Mo^{V}_2O_4]^{2+}$ as reducing Mo species.

However, if hydrazine hydrate was not added during the synthesis, only "Trojan Horse" type clusters $[W_{18}O_{56}(HPO_3)_2(H_2O)_2]^{8-}$ [7] formed as the exclusive product. Similarly, if sodium molybdate dihydrate was absent, the initially reduced solution of tungstate will

be gradually oxidized during the crystallization and gave rise to "Trojan Horse" type clusters $[W_{18}O_{56}(HPO_3)_2(H_2O)_2]^{8-}$ as well. Therefore, the presence of reduced Mo species is essential for the formation of compounds **1**-**10**. The control experiments and original synthesis of **4** are summarized in Scheme S1 for a clearer comparison.

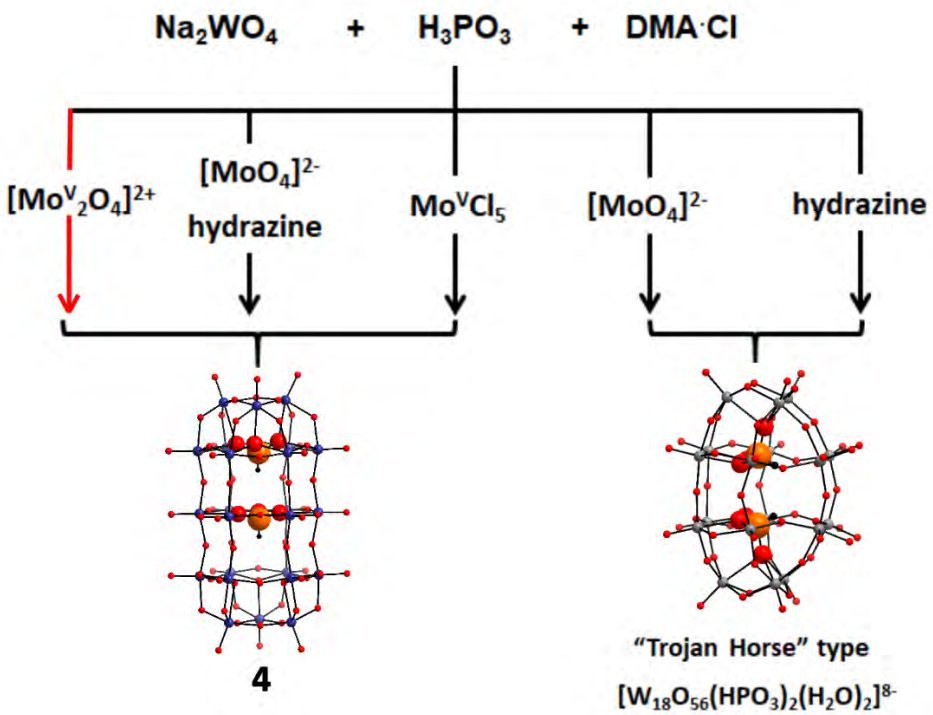

Scheme S1. Schematic representation of the original synthesis of compound **4** and control experiments, showing the key role of the reduced Mo species in directing the self-assembly of multi-layered POM clusters. The original synthesis of **4** is emphasized by the red arrow, and the control experiments are indicated by the black arrows. Colour scheme: orange: P; indigo: W/Mo^V; grey: W; red: O; black: hydrogen.

3. Single-crystal X-ray structure determination

Table S1 Crystal data and structure refinement for compound 1-3.

Identification code	**1**	**2**	**3**
Empirical formula	$C_{14}H_{90}Mo_2N_7O_{75}PW_{16}$	$C_{14}H_{79}Mo_2N_7O_{70}SeW_{16}$	$C_{14}H_{79}Mo_2N_7O_{70}TeW_{16}$
Formula weight	4721.37	4678.28	4726.92
Temperature	150(2) K	150(2) K	150(2) K
Wavelength	0.71073 Å	0.71073 Å	71.073 Å
Crystal system	Trigonal	Trigonal	Trigonal
Space group	R -3 m :H	R -3 m :H	R -3 m :H
Unit cell dimensions	a = 21.5987(10) Å	a = 21.1690(9) Å	a = 21.1678(9) Å
	b = 21.5987(10) Å	b = 21.1690(13) Å	b = 21.1678(9) Å
	c = 13.9195(15) Å	c = 15.8379(12) Å	c = 15.6954(14) Å
Volume	5623.5(8) Å ^{3}	6146.5(7) Å ^{3}	6090.5(8) Å ^{3}
Z	3	3	3
Density (calculated)	4.182 Mg/m^3	3.792 Mg/m^3	3.866 Mg/m^3
Absorption coefficient	24.903 mm^{-1}	23.200 mm^{-1}	23.317 mm^{-1}
F(000)	6318	6222	6276
Crystal size	0.070 x 0.050 x 0.030 mm^3	0.100 x 0.050 x 0.050 mm^3	0.100 x 0.050 x 0.050 mm^3
θ range for data collection	1.824 to 26.998°.	2.802 to 25.994°.	2.573 to 25.723°.
Index ranges	-15<=h<=23, -15<=k<=27, -17<=l<=17	-26<=h<=16, -21<=k<=24, -19<=l<=18	-25<=h<=23, -25<=k<=25, -19<=l<=19
Reflections collected	6807	7799	28942
Independent reflections	1450 [R(int) = 0.0807]	1459 [R(int) = 0.0493]	1408 [R(int) = 0.0553]
Completeness to θ 25°	100.0 %	99.7 %	99.9 %
Absorption correction	Empirical	Empirical	Empirical
Max. & min. transmission	0.0942 and 0.0376	0.093 and 0.057	0.547 and 0.216
Refinement method	Full-matrix least-squares on F^2	Full-matrix least-squares on F^2	Full-matrix least-squares on F^2
Data/restraints/parameters	1450 / 5 / 86	1459 / 4 / 100	1408 / 2 / 86
Goodness-of-fit on F^2	1.118	1.121	1.237
Final R indices [I>2σ(I)]	R1 = 0.0487, wR2 = 0.1238	R1 = 0.0390, wR2 = 0.0895	R1 = 0.0399, wR2 = 0.1108
R indices (all data)	R1 = 0.0720, wR2 = 0.1368	R1 = 0.0563, wR2 = 0.1010	R1 = 0.0525, wR2 = 0.1234
Extinction coefficient	n/a	n/a	n/a
Largest diff. peak and hole	3.97 and -2.97 e.Å^{-3}	1.07 and -2.22 e.Å^{-3}	1.81 and -2.39 e.Å^{-3}

Table S2 Crystal data and structure refinement for compound 4-6.

Identification code	**4**	**6**
Empirical formula	$C_{20}H_{113}Mo_3N_{10}Na_2O_{96}P_2W_{21}$	$C_{22}H_{119}Mo_3N_{11}NaO_{96}Se_2W_{21}$
Formula weight	6286.79	6403.85
Temperature	150(2) K	150(2) K
Wavelength	0.71073 Å	0.71073 Å
Crystal system	Orthorhombic	Orthorhombic
Space group	P n m a	P n m a
Unit cell dimensions	a = 35.244(2) Å	a = 20.577(2) Å
	b = 21.9528(13) Å	b = 21.446(2) Å
	c = 15.0516(8) Å	c = 25.391(3) Å
Volume	11645.4(11) $Å^3$	11204.7(19) $Å^3$
Z	4	4
Density (calculated)	3.586 Mg/m^3	3.796 Mg/m^3
Absorption coefficient	21.099 mm^{-1}	22.548 mm^{-1}
F(000)	11212	11420
Crystal size	0.100 x 0.060 x 0.050 mm^3	0.100 x 0.050 x 0.050 mm^3
θ range for data collection	1.640 to 25.999°.	1.243 to 26.000°.
Index ranges	-43<=h<=43, -27<=k<=25, -18<=l<=18	-25<=h<=25, -26<=k<=26, -31<=l<=31
Reflections collected	166812	168417
Independent reflections	11754 [R(int) = 0.0787]	11330 [R(int) = 0.0579]
Completeness to θ 25°	99.9 %	99.9 %
Absorption correction	Empirical	Empirical
Max. & min. transmission	0.0223 and 0.0091	0.062 and 0.012
Refinement method	Full-matrix least-squares on F^2	Full-matrix least-squares on F^2
Data/restraints/parameters	11754 / 112 / 663	11330 / 530 / 676
Goodness-of-fit on F^2	1.193	1.258
Final R indices [I>2σ(I)]	R1 = 0.1167, wR2 = 0.2465	R1 = 0.0754, wR2 = 0.1888
R indices (all data)	R1 = 0.1443, wR2 = 0.2791	R1 = 0.0966, wR2 = 0.2179
Extinction coefficient	n/a	n/a
Largest diff. peak and hole	5.59 and -9.76 $e.Å^{-3}$	3.37 and -3.25 $e.Å^{-3}$

Table S3 Crystal data and structure refinement for compound 7-8.

Identification code	**7**	**8**
Empirical formula	$C_{20}H_{112}Mo_2N_{10}NaO_{96}PSeW_{22}$	$C_{22}H_{120}Mo_3N_{11}NaO_{96}PTeW_{21}$
Formula weight	6398.69	6405.51
Temperature	150(2) K	150(2) K
Wavelength	0.71073 Å	0.71073 Å
Crystal system	Cubic	Orthorhombic
Space group	P a -3	P n m a
Unit cell dimensions	a = 22.5570(18) Å	a = 35.220(3) Å
	b = 22.5570(18) Å	b = 22.1684(19) Å
	c = 22.5570(18) Å	c = 15.0386(11) Å
Volume	11477(3) $Å^3$	11741.7(16) $Å^3$
Z	4	4
Density (calculated)	3.703 Mg/m^3	3.624 Mg/m^3
Absorption coefficient	22.599 mm^{-1}	21.154 mm^{-1}
F(000)	11368	11420
Crystal size	0.149 x 0.070 x 0.068 mm^3	0.089 x 0.084 x 0.057 mm^3
θ range for data collection	2.019 to 25.995°.	1.636 to 25.500°.
Index ranges	-27<=h<=27, -27<=k<=27, -27<=l<=27	-42<=h<=42, -26<=k<=26, -18<=l<=18
Reflections collected	161282	166207
Independent reflections	3776 [R(int) = 0.0583]	11238 [R(int) = 0.0699]
Completeness to θ 25°	99.9 %	99.9 %
Absorption correction	Empirical	Empirical
Max. & min. transmission	0.0309 and 0.0072	0.0235 and 0.0083
Refinement method	Full-matrix least-squares on F^2	Full-matrix least-squares on F^2
Data/restraints/parameters	3776 / 10 / 212	11238 / 510 / 703
Goodness-of-fit on F^2	1.214	1.203
Final R indices [I>2σ(I)]	R1 = 0.0794, wR2 = 0.2043	R1 = 0.1084, wR2 = 0.2465
R indices (all data)	R1 = 0.1004, wR2 = 0.2389	R1 = 0.1200, wR2 = 0.2562
Extinction coefficient	n/a	n/a
Largest diff. peak and hole	1.99 and -1.73 $e.Å^{-3}$	4.38 and -5.98 $e.Å^{-3}$

Table S4 Crystal data and structure refinement for compound 9-11.

Identification code	**9**	**10**	**11**
Empirical formula	$C_{32}H_{161}Mo_4N_{16}O_{117}P_3W_{26}$	$C_{60}H_{291}Mo_4N_{30}NaO_{251}Se_7W_{62}$	$C_{80}H_{183}Mo_2N_5O_{60}TeW_{16}$
Formula weight	7899.53	17808.38	5436.38
Temperature	150(2) K	150(2) K	150(2) K
Wavelength	0.71073 Å	0.71073 Å	0.71073 Å
Crystal system	Orthorhombic	Triclinic	Trigonal
Space group	C m c a	P -1	R -3 :H
Unit cell dimensions	a = 21.7592(18) Å	a = 17.7735(13) Å	a = 44.713(3) Å
	b = 26.906(2) Å	b = 20.1721(14) Å	b = 44.713(3) Å
	c = 25.728(2) Å	c = 22.3319(16) Å	c = 47.217(5) Å
		α= 99.133(4)°.	
		β= 102.654(4)°.	
		γ = 96.166(4)°.	
Volume	15062(2) $Å^3$	7628.6(10) $Å^3$	81751(14) $Å^3$
Z	4	1	24
Density (calculated)	3.484 Mg/m^3	3.876 Mg/m^3	2.650 Mg/m^3
Absorption coefficient	20.221 mm^{-1}	24.365 mm^{-1}	13.911 mm^{-1}
F(000)	14152	7874	59952
Crystal size	0.100 x 0.100 x 0.100 mm^3	0.100 x 0.050 x 0.050 mm^3	0.100 x 0.100 x 0.060 mm^3
θ range for data collection	1.872 to 26.449°.	1.455 to 26.000°.	0.680 to 23.298°.
Index ranges	-25<=h<=27, -33<=k<=30, -30<=l<=32	-21<=h<=19, -24<=k<=24, -27<=l<=26	-49<=h<=46, -49<=k<=49, -52<=l<=52
Reflections collected	61753	115963	122591
Independent reflections	7946 [R(int) = 0.0429]	29949 [R(int) = 0.0503]	23878 [R(int) = 0.0818]
Completeness to θ 25°	99.9 %	99.9 %	91.0 %
Absorption correction	Empirical	Analytical	Empirical
Max. & min. transmission	0.0085 and 0.0020	0.0526 and 0.0122	0.0886 and 0.0378
Refinement method	Full-matrix least-squares on F^2	Full-matrix least-squares on F^2	Full-matrix least-squares on F^2
Data/restraints/parameters	7946 / 30 / 439	29949 / 72 / 1634	23878 / 43 / 1149
Goodness-of-fit on F^2	1.184	1.095	1.075
Final R indices [I>2σ(I)]	R1 = 0.0514, wR2 = 0.1393	R1 = 0.0569, wR2 = 0.1465	R1 = 0.0772, wR2 = 0.2088
R indices (all data)	R1 = 0.0766, wR2 = 0.1804	R1 = 0.0903, wR2 = 0.1755	R1 = 0.1430, wR2 = 0.2747
Extinction coefficient	n/a	n/a	n/a
Largest diff. peak and hole	2.27 and -2.18 $e.Å^{-3}$	3.73 and -5.32 $e.Å^{-3}$	2.49 and -1.71 $e.Å^{-3}$

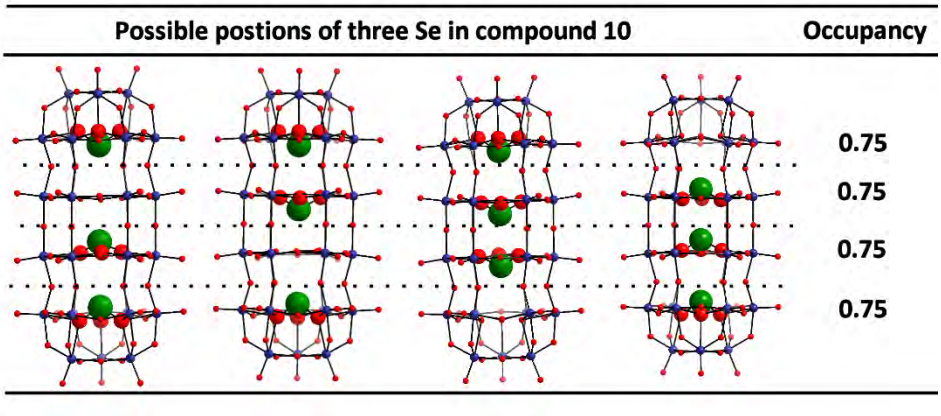

Figure S1. Three selenium atoms disordered in four heteroatom positions in compound **10,** with a 0.75 occupancy in each position.

4. UV-Vis-NIR spectroscopy

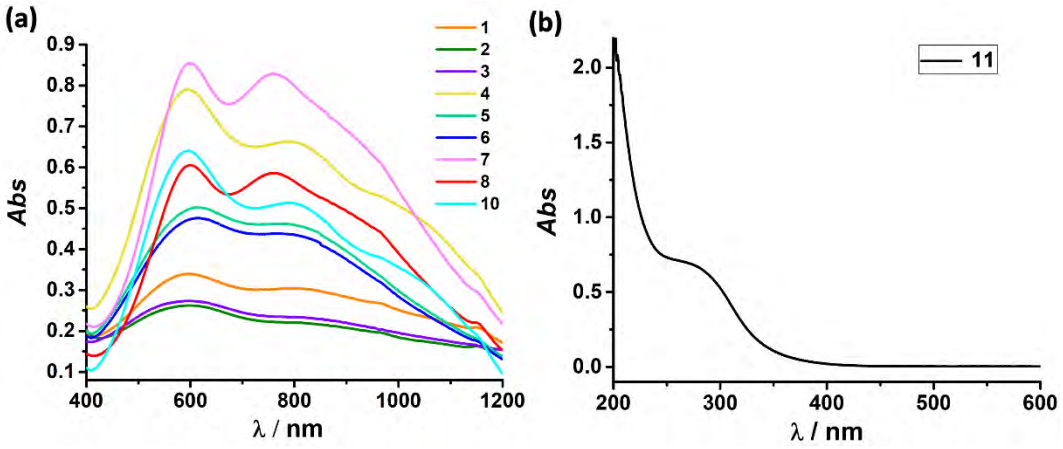

Figure S2. UV-vis-NIR spectroscopy of a) compound **1**-**8**, **10** and b) compound **11**.

5. ESI-mass spectrometry

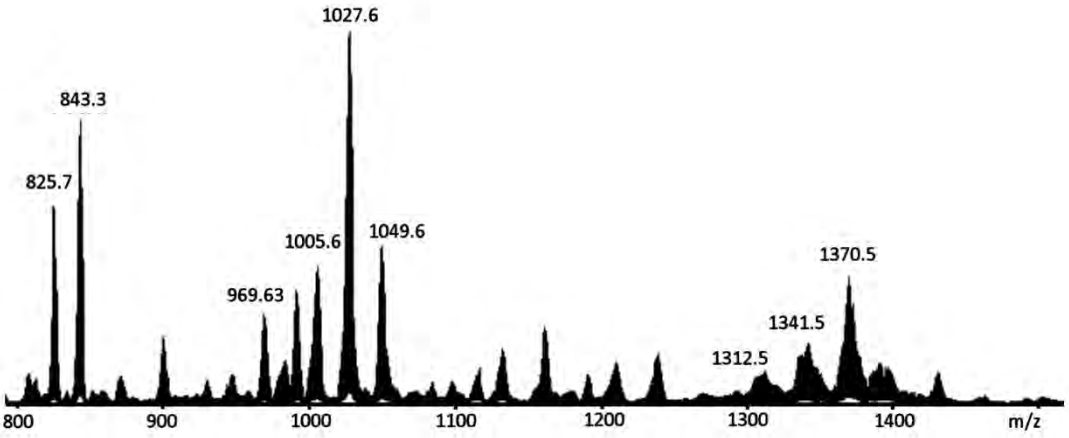

Figure S3. ESI-MS spectra of **1** in water/acetonitrile (5 %:95 %) mixture solvent.

Table S5. Mass spectral analysis of **1** in water/acetonitrile (5%:95%) mixture solvent, with proposed formula and charge of peaks.

z	m/z (obs)	m/z (cal)	Assignment

5-	825.7	825.6	$HPW_{16}Mo_2O_{60}H_3$
	843.3	843.2	$HPW_{17}Mo_1O_{60}H_3$
4-	983.6	983.2	$HPW_{13}Mo_5O_{60}(C_2H_8N)_1Na_1H_2$
	991.6	992.2	$HPW_{13}Mo_5O_{60}(C_2H_8N)_1Na_1H_2(H_2O)$
	1005.6	1005.2	$HPW_{14}Mo_4O_{60}(C_2H_8N)_1Na_1H_2$
	1027.6	1027.2	$HPW_{15}Mo_3O_{60}(C_2H_8N)_1Na_1H_2$
	1049.6	1048.9	$HPW_{16}Mo_2O_{60}(C_2H_8N)_1Na_1H_2$
3-	1312.5	1311.9	$HPW_{12}Mo_6O_{60}(C_2H_8N)_3Na_1H_1$
	1341.5	1341.3	$HPW_{13}Mo_5O_{60}(C_2H_8N)_3Na_1H_1$
	1370.5	1370.6	$HPW_{14}Mo_4O_{60}(C_2H_8N)_3Na_1H_1$

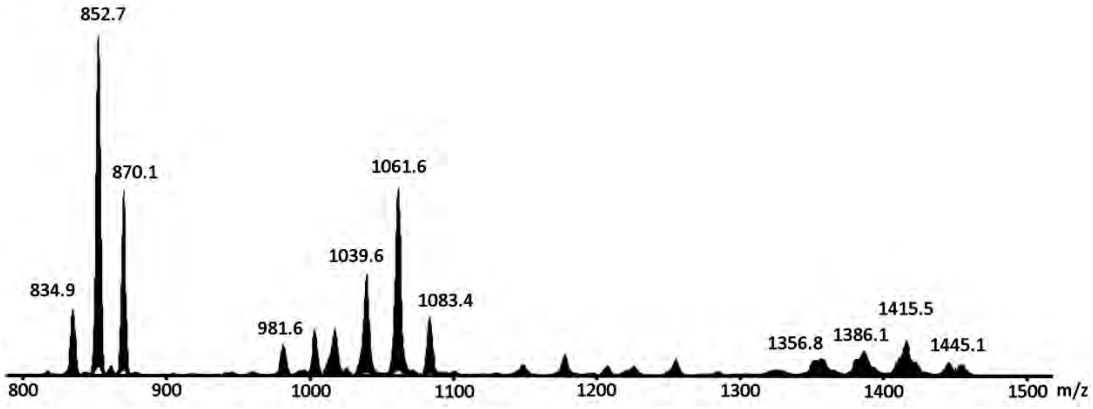

Figure S4. ESI-MS spectra of **2** in water/acetonitrile (5 %:95 %) mixture solvent.

Table S6. Mass spectral analysis of **2** in water/acetonitrile (5 %:95 %) mixture solvent, with proposed formula and charge of peaks

z	m/z (obs)	m/z (cal)	Assignment
5-	834.9	835.1	$SeW_{16}Mo_2O_{60}H_3$
	852.7	853.1	$SeW_{16}Mo_2O_{60}(C_2H_8N)_2H_1$
	870.1	869.4	$SeW_{16}Mo_2O_{60}(C_2H_8N)_3(H_2O)_2$
4-	981.6	982.6	$SeW_{13}Mo_5O_{60}H_4(H_2O)_1$
	1003.6	1004.6	$SeW_{13}Mo_5O_{60}Na_4(H_2O)_1$
	1017.6	1016.9	$SeW_{14}Mo_4O_{60}(C_2H_8N)_1Na_1H_2$
	1039.6	1038.9	$SeW_{15}Mo_3O_{60}(C_2H_8N)_1Na_1H_2$
	1061.6	1060.9	$SeW_{16}Mo_2O_{60}(C_2H_8N)_1Na_1H_2$
	1083.4	1083.5	$SeW_{16}Mo_2O_{60}(C_2H_8N)_3Na_1$
3-	1303.5	1304.5	$SeW_{13}Mo_5O_{60}H_5$
	1322.4	1323.8	$SeW_{13}Mo_5O_{60}Na_1H_4(H_2O)_2$
	1327.4	1326.5	$SeW_{13}Mo_5O_{60}Na_3H_2$
	1352.1	1353.2	$SeW_{14}Mo_4O_{60}Na_4H_1(H_2O)_2$
	1356.8	1356.2	$SeW_{14}Mo_4O_{60}(C_2H_8N)_1Na_1H_3$
	1381.8	1382.5	$SeW_{15}Mo_3O_{60}(C_2H_8N)_1Na_1H_4(H_2O)_2$
	1386.1	1385.6	$SeW_{15}Mo_3O_{60}(C_2H_8N)_1Na_1H_3$
	1415.5	1415.6	$SeW_{15}Mo_3O_{60}(C_2H_8N)_3Na_1H_1$
	1445.1	1445.0	$SeW_{16}Mo_2O_{60}(C_2H_8N)_3Na_1H_1$

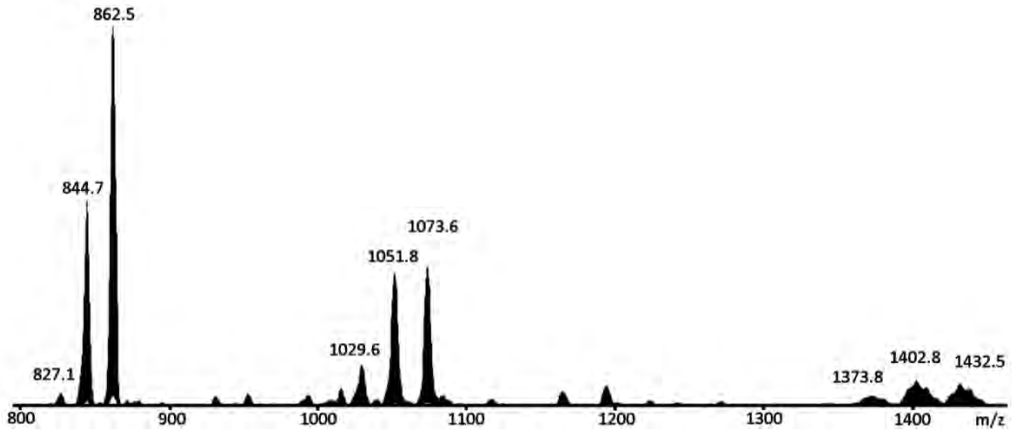

Figure S5. ESI-MS spectra of **3** in water/acetonitrile (5%:95%) mixture solvent.

Table S7. Mass spectral analysis of **3** in water/acetonitrile (5%:95%) mixture solvent, with proposed formula and charge of peaks

z	m/z (obs)	m/z (cal)	Assignment

	827.1	827.1	$TeW_{15}Mo_3O_{60}H_3$
5-	844.7	845.1	$TeW_{15}Mo_3O_{60}(C_2H_8N)_2H_1$
	862.5	862.7	$TeW_{16}Mo_2O_{60}(C_2H_8N)_2H_1$
	993.6	994.9	$TeW_{13}Mo_5O_{60}H_4(H_2O)$
	1015.4	1016.9	$TeW_{14}Mo_4O_{60}H_4(H_2O)$
4-	1029.6	1029.1	$TeW_{14}Mo_4O_{60}(C_2H_8N)_1Na_1H_2$
	1051.8	1051.7	$TeW_{14}Mo_4O_{60}(C_2H_8N)_3Na_1$
	1073.6	1073.4	$TeW_{14}Mo_4O_{60}(C_2H_8N)_3Na_1$
	1362.1	1363.5	$TeW_{14}Mo_4O_{60}Na_1H_4(H_2O)_1$
	1373.8	1372.6	$TeW_{14}Mo_4O_{60}(C_2H_8N)_1Na_1H_3$
	1379.4	1379.2	$TeW_{14}Mo_4O_{60}H_5$
	1397.4	1398.5	$TeW_{15}Mo_3O_{60}Na_1H_4(H_2O)_2$
3-	1402.8	1401.5	$TeW_{15}Mo_3O_{60}(C_2H_8N)_1Na_1H_3$
	1409.1	1409.2	$TeW_{15}Mo_3O_{60}(C_2H_8N)_2H_3$
	1427.4	1427.9	$TeW_{16}Mo_2O_{60}Na_1H_4(H_2O)_2$
	1432.5	1432.6	$TeW_{16}Mo_2O_{60}H_5(H_2O)_4$
	1438.5	1438.6	$TeW_{16}Mo_2O_{60}(C_2H_8N)_2H_3$
	1444.8	1445.9	$TeW_{16}Mo_2O_{60}(C_2H_8N)_2Na_1H_2$

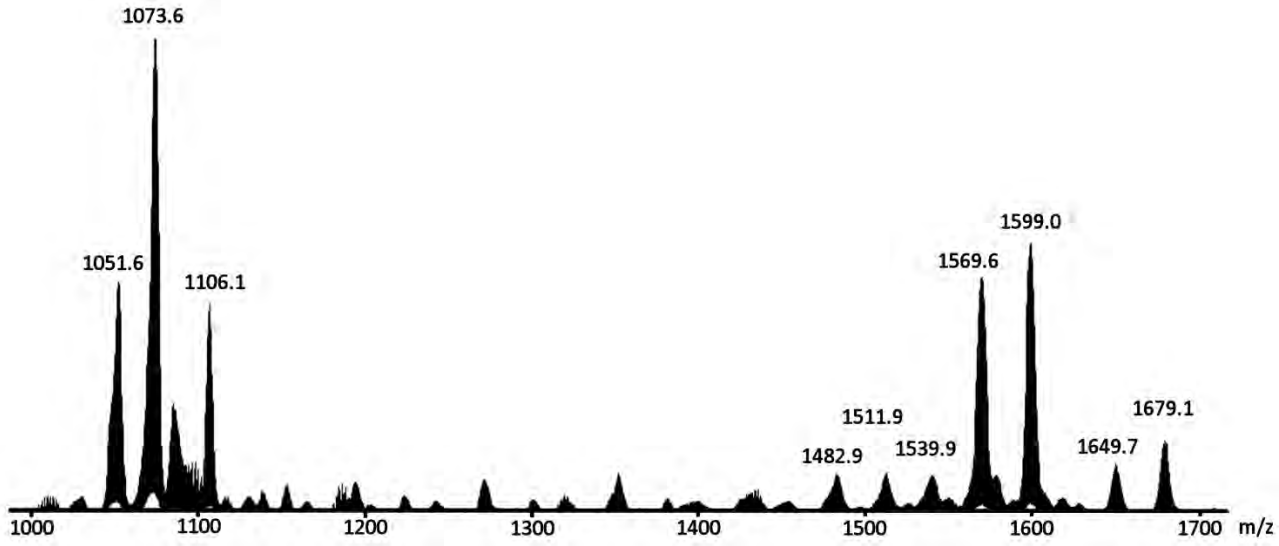

Figure S6. ESI-MS spectra of **11** in acetonitrile.

Table S8. Mass spectral analysis of **11** in acetonitrile with proposed formula and charge of peaks

z	m/z (obs)	m/z (cal)	Assignment
	1679.01	1679.5	$(TeW_{17}Mo_1O_{60})(C_{16}H_{36}N)_3H_2$
	1649.7	1650.2	$(TeW_{16}Mo_2O_{60})(C_{16}H_{36}N)_3H_2$
	1599.0	1598.7	$(Te_1W_{17}Mo_1O_{60})(C_{16}H_{36}N)_2H_3$
-3	1570.0	1569.4	$(TeW_{16}Mo_2O_{60})(C_{16}H_{36}N)_2H_3$
	1539.9	1540.4	$(Te_1W_{15}Mo_3O_{60})(C_{16}H_{36}N)_2H_3$
	1511.9	1511.0	$(Te_1W_{14}Mo_4O_{60})(C_{16}H_{36}N)_2H_3$
	1482.9	1481.7	$(Te_1W_{13}Mo_5O_{60})(C_{16}H_{36}N)_2H_3$
	1138.4	1138.5	$(Te_1W_{17}Mo_1O_{60})(C_{16}H_{36}N)_1H_3$
	1106.1	1107.4	$(Te_1W_{16}Mo_2O_{60})H_4(CH_3CN)_5$
-4	1084.9	1085.7	$(Te_1W_{15}Mo_3O_{60})H_4(CH_3CN)_5$
	1073.6	1072.7	$(Te_1W_{14}Mo_4O_{60})(C_{16}H_{36}N)_1H_3$
	1051.3	1051.0	$(Te_1W_{13}Mo_5O_{60})(C_{16}H_{36}N)_1H_3$

6. NMR study

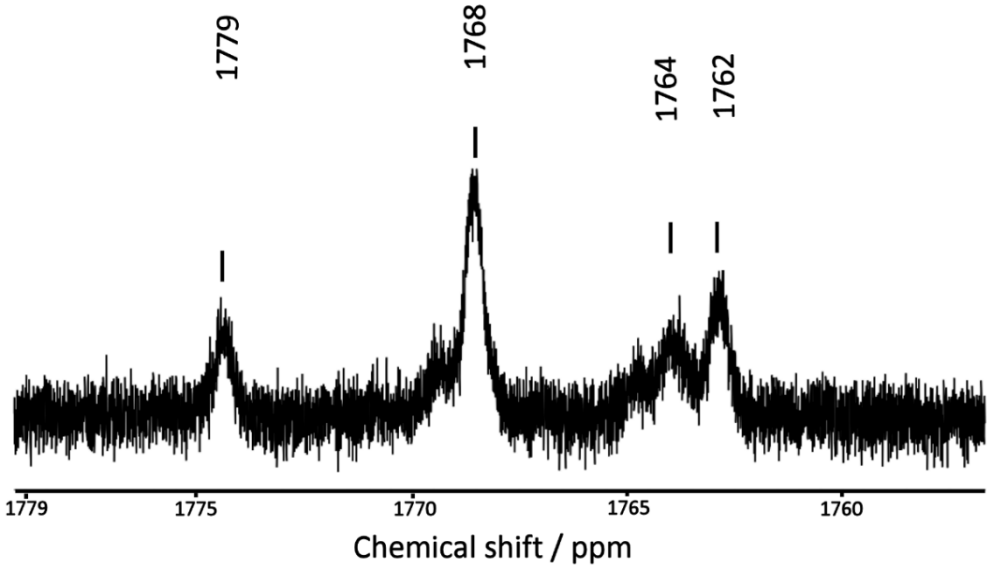

Figure S7. ^{125}Te NMR spectrum of **11** in dimethyl sulfoxide-d_6.

7. Dielectric property

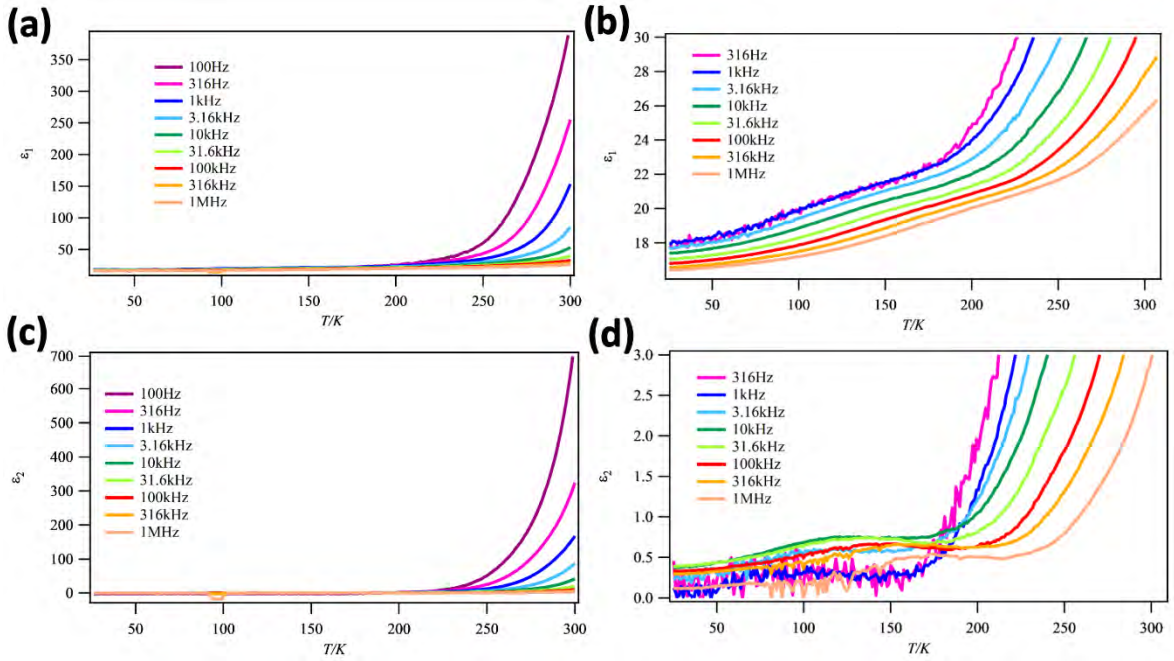

Figure S8. Temperature dependence of real ε_1 (a and b) and imaginary ε_2 (c and d) parts of the complex dielectric constant for **4**, characterized by the impedance method in the frequency range from 100 Hz to 1 MHz and were plotted.

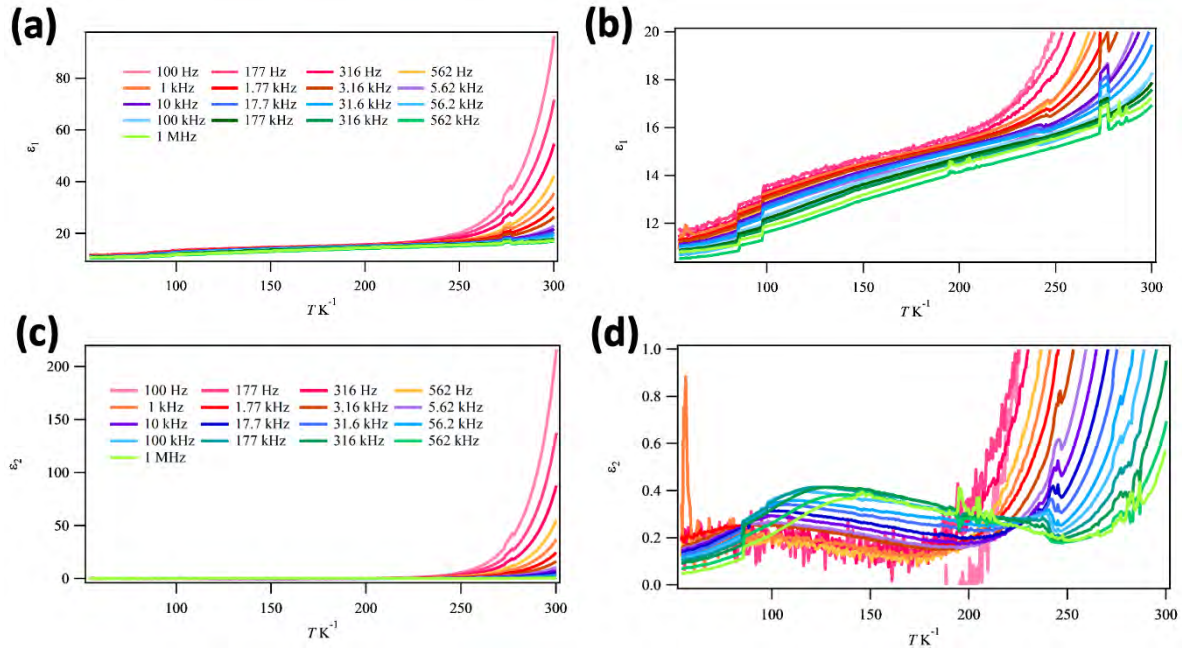

Figure S9. Temperature dependence of real ε_1 (a and b) and imaginary ε_2 (c and d) parts of the complex dielectric constant for **6**, characterized by the impedance method in the frequency range from 100 Hz to 1 MHz and were plotted.

8. TGA analysis

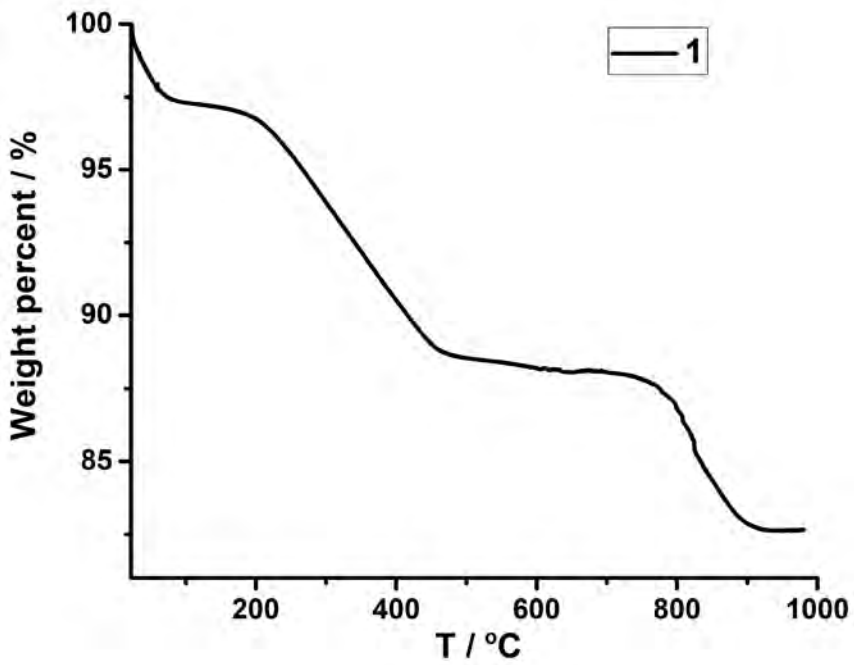

Figure S10. TGA curve for compound **1**.

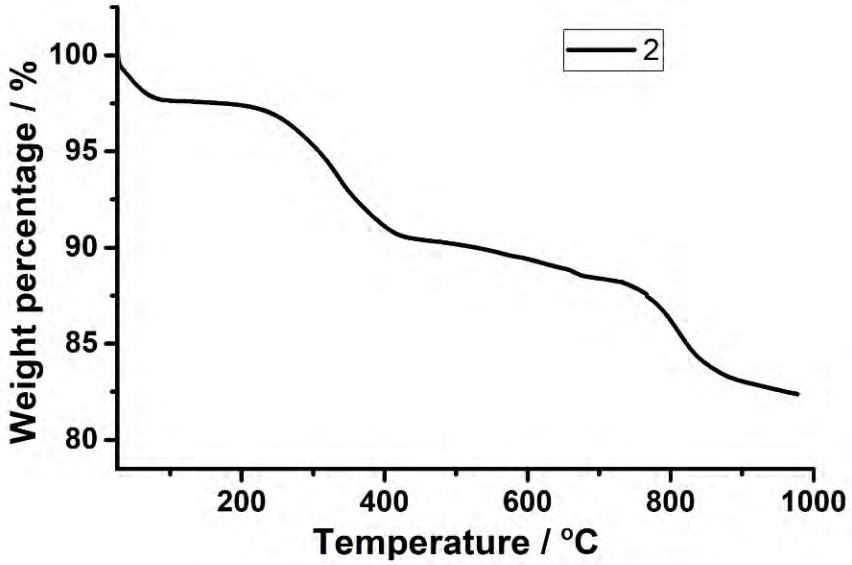

Figure S11. TGA curve for compound **2**.

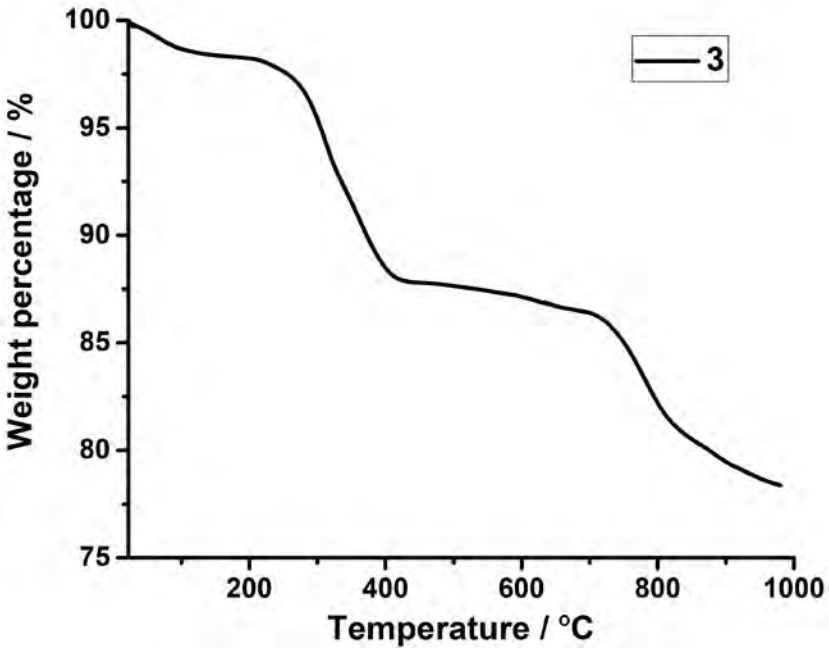

Figure S12. TGA curve for compound **3**.

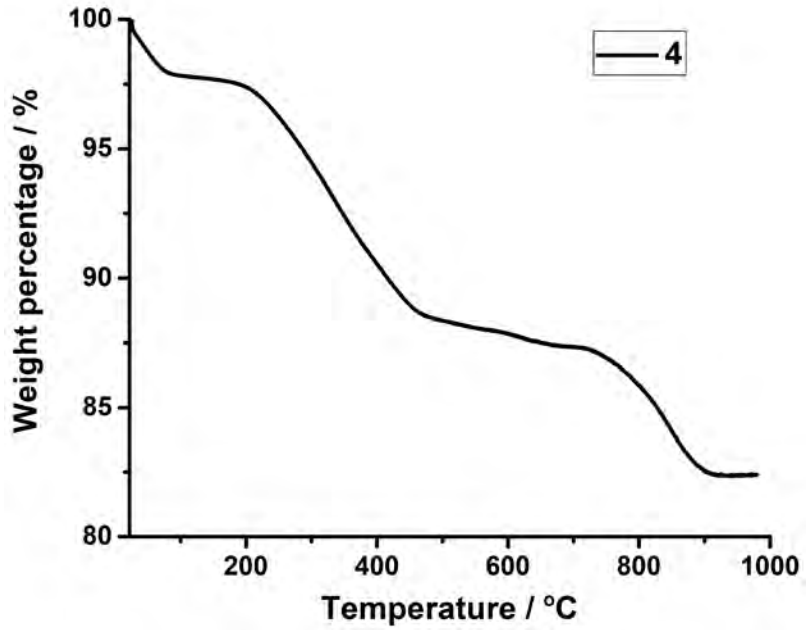

Figure S13. TGA curve for compound **4**.

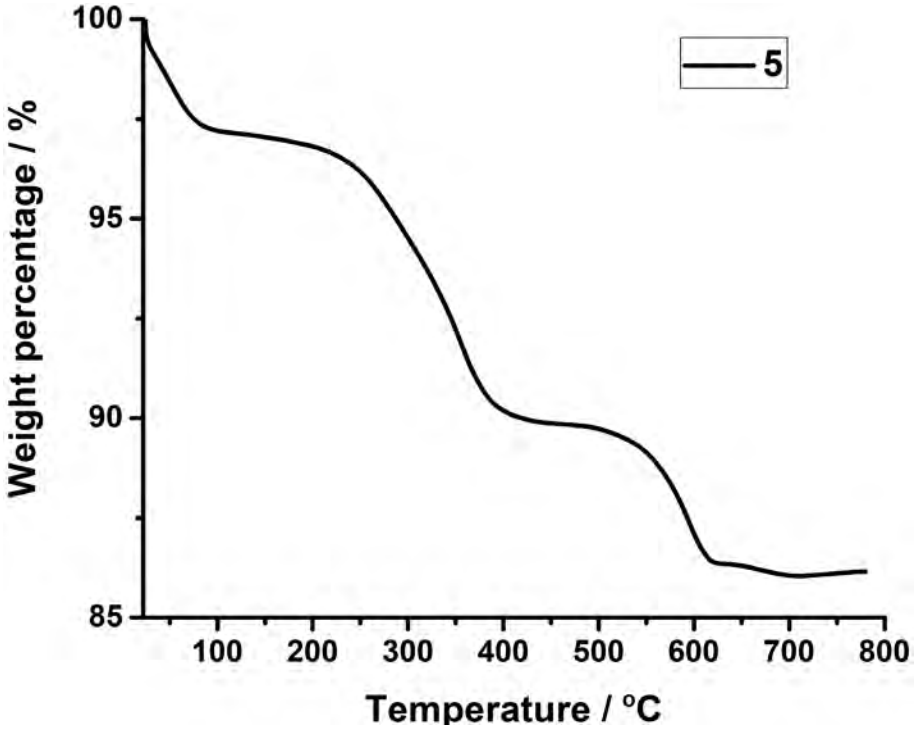

Figure S14. TGA curve for compound **5**.

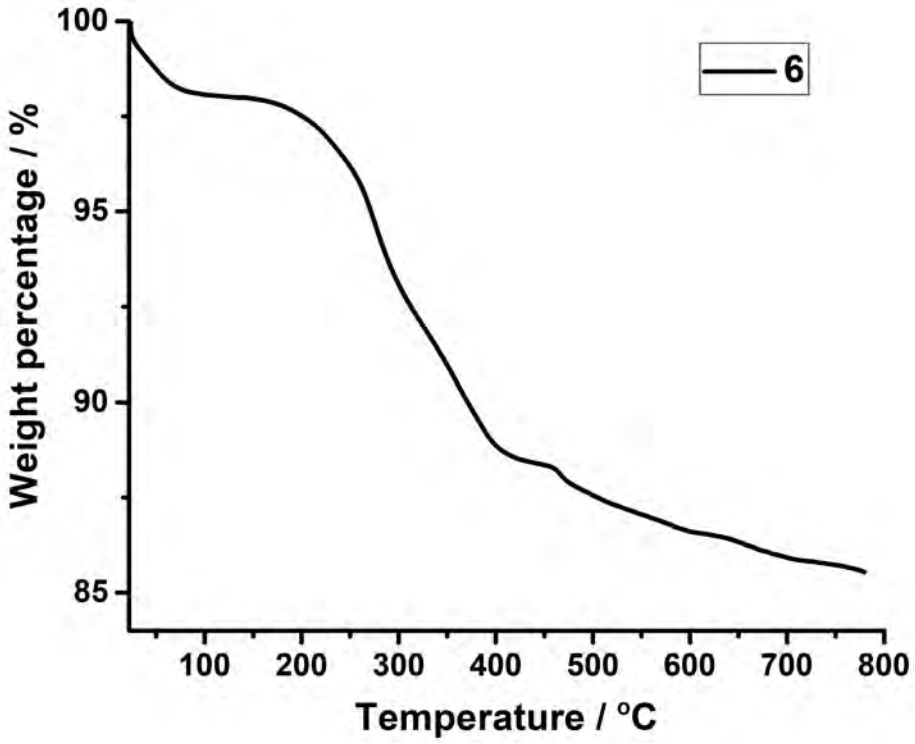

Figure S15. TGA curve for compound **6**.

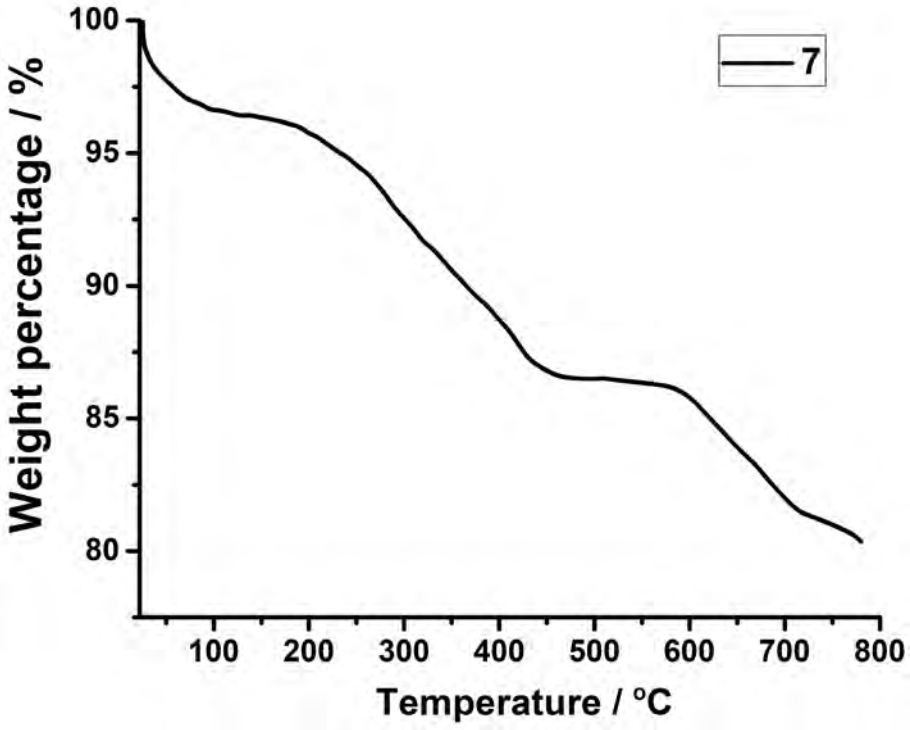

Figure S16. TGA curve for compound **7**.

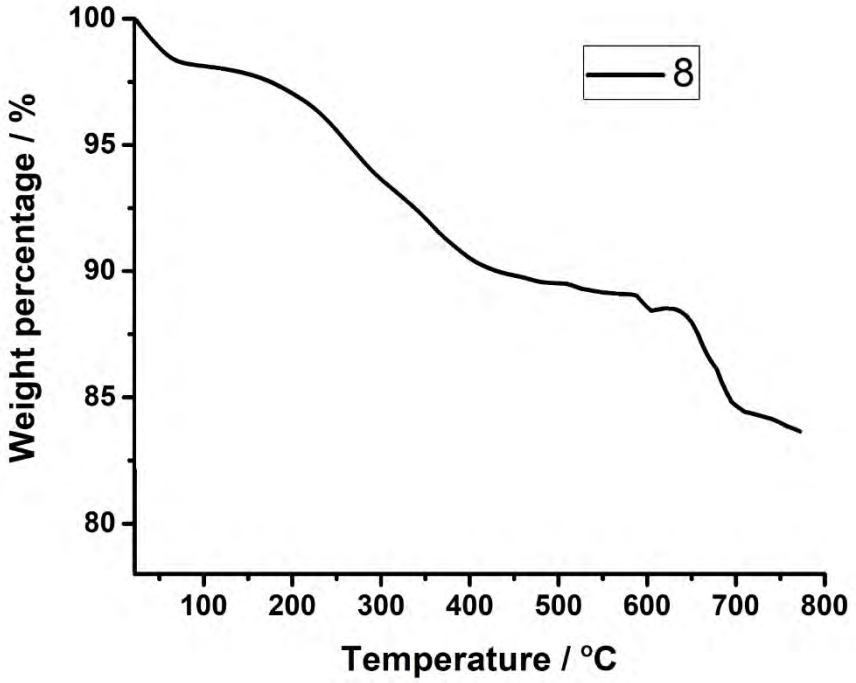

Figure S17. TGA curve for compound **8**.

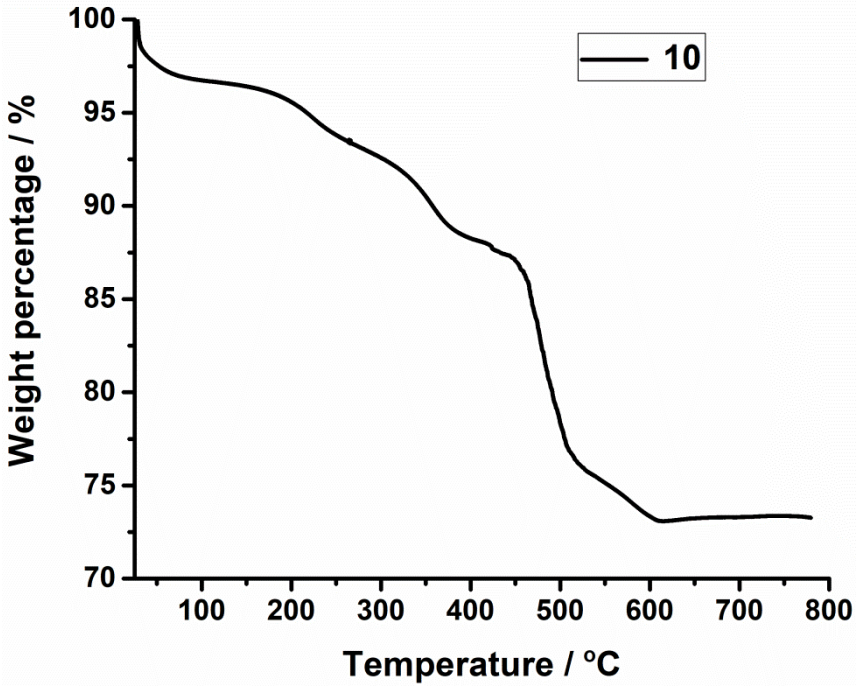

Figure S18. TGA curve for compound **10**.

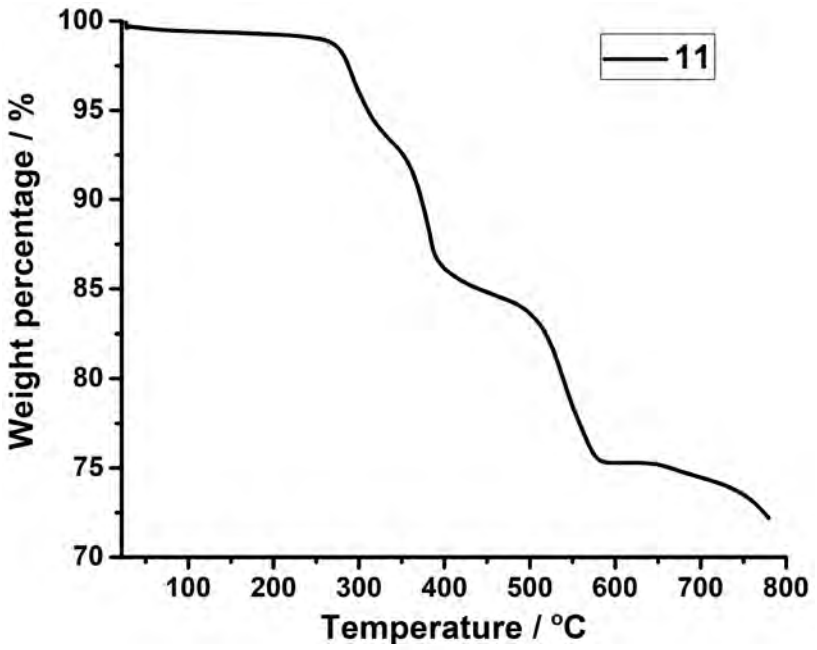

Figure S19. TGA curve for compound **11**.

9. Redox titrations

The cerimetric titration was carried out using a 0.0025 M solution of Ce^{IV} in 0.5 M of sulphuric acid as oxidant which was added dropwise to a solution of compound **1** (19.2 mg in 20 mL of H_2O). After addition of 3.1 mL of the oxidant the colour of the solution turned from deep blue to light yellow along with a characteristic potential jump showed the presence of 1.82 e^- which (formally) corresponds to 2 Mo^V centers (theoretical value for 2 e^- reduced species: 3.4 mL). The cerimetric titration of all the samples were performed in the same way, and the results are summarized as follows:

Compound	Concentration (mg/50mL)	Number of electrons	Volume of the oxidant (*obs*) (mL)	Volume of the oxidant (*cal*) (mL)
1	19.2	2	3.1	3.4
2	34.8	2	5.9	6.0
3	30.0	2	4.9	5.1
4	26.0	3	5.2	4.9
5	26.0	3	5.2	4.9
6	26.0	2	3.4	3.4
7	26.0	2	3.5	3.2
8	18.0	3	3.2	3.4
10	16.0	4	1.5	1.4

10. Reference

[1] G. Sheldrick, *AcataCrystallogr. Sect. A*. **1990**, *46*, 467-473.
[2] G. Sheldrick, *ActaCrystallogr. Sect. A*, **2008**, *64*, 112-122.
[3] L. Farrugia, *J. Appl. Crystallogr.* **1999**, *32*, 837-838.
[4] R. C. Clark, J. S. Reid, *ActaCrystallogr. Sect. A*. **1995**, *51*, 887–897.
[5] A. Dolbecq, J.-D. Compain, P. Mialane, J. Marrot, F. Secheresse, B. Keita, L. Roberto Brudna Holzle, F. Miserque, L. Nadjo, *Chem. Eur. J.* **2009**, *15*, 733-741.
[6] C. Busche, L. Vilà-Nadal, J. Yan, H. N. Miras, D.-L. Long, V. P. Georgiev, A. Asenov, R. H. Pedersen, N. Gadegaard, M. M. Mirza, D. J. Paul, J. M. Poblet, L. Cronin, *Nature* **2014**, *515*, 545–549.
[7] Q. Zheng, L. Vilà-Nadal, C. Busche, J. S. Mathieson, D.-L. Long, L. Cronin, *Angew. Chemie* **2015**, *127*, 8006-8010; *Angew. Chem. Int. Ed.* ***2015***, 54, 7895-7899